MSc Thesis

Performing Visual Field Examinations using a Virtual Reality Headset: An Explorative Study

General information

Location: Amsterdam University Medical Centre
Department: Department of Neurosurgery
Start date: 16-01-2023
End date: 28-08-2024
Course: TM30004 – TM MSc Thesis
Track: Sensing & Stimulation

Student

Name: Marloes Krista van der Werf
StudentID: 4334140

Medical supervision

Name: S. Idema
Function: Neurosurgeon

Technical supervision

Name: J.J. Van den Dobbelsteen
Function: Director of studies Technical Medicine

Performing Visual Field Examinations using a Virtual Reality Headset: An Explorative Study

TM30004 MSc Thesis

Marloes van der Werf, 4334140
Department of Neurosurgery, Amsterdam University Medical Center

August 28, 2024

Thesis in partial fulfilment for the joint degree of Master in Science in

Technical Medicine

Leiden University — Delft University of Technology — Erasmus University Rotterdam

Supervisors:

Prof. Dr. John van den Dobbelsteen
Dr. Sander Idema

Thesis committee members:

Chair/technical supervisor: Prof.dr. J.J. van den Dobbelsteen
Medical supervisor: Dr. S. Idema
Independent member: Prof.dr.ir. J. Harlaar

An electronic version of this thesis is available at:

`http://repository.tudelft.nl` s

Table of Contents

Abbreviations

VR(H)	Virtual Reality (Headset)
HMD	Head Mounted Display
3D	Three dimensional
OR	Operating Room
ET(T)	Eye-tracking (Technology)
QoL	Quality of life

Abstract

Background Over the past few years, virtual reality-based visual field assessments have been increasingly investigated. However, due to the limited field of view (FOV) that a virtual reality (VR) headset can offer, research to identify the visual field's outer limits has not been possible as the FOV falls short of the human visual field limits. This limitation has hindered the ability to accurately identify the outer limits of the visual field using VR technology. The Peili Research app, a VR-based kinetic perimeter, addresses this issue by employing off-centred focus points to expand the effective angle that can be tested.

Research Objective This research explores the feasibility of employing the Peili Research app, alongside the Pico Neo 2 Eye VR headset, as a bedside tool for visual field assessment.

Methods A series of analyses were conducted to evaluate the Peili Research app's performance in visual field testing. The Spearman correlation matrix was used to assess test-retest reliability, and a comparison with Goldmann perimetry was made. The app's design was evaluated by calculating the increase in effective testable angle through the off-centred focus point. In addition, the impact of observer differences due to human reaction time and the impact of stimulus colour contrast on the results was investigated. Data processing was conducted using a custom-developed MATLAB script to analyse the Peili data and determine the visual field angles in isopters.

Results Visual representations of the Peili Research app suggested a certain extent of test-retest reliability. However, Spearman correlations varied between poor and moderate. The application extends the testable visual field angle by 23 degrees on average. The study revealed that human reaction time in recording visual stimuli on the tablet led to an average underestimation of visual field angles by 5.38 degrees ($p<0.001$). Furthermore, colour contrast significantly affected detection angles, with green stimuli being detected at larger angles compared to blue and yellow stimuli ($p<0.001$). Clinical testing on postoperative volunteers highlighted practical challenges.

Conclusion The Peili Research app shows promise as a VR-based tool for visual field assessment, capable of expanding the testable visual field angle. However, variability in results, mainly due to the location of the focus points, reaction time, colour contrast, and the instability of the VR headset, highlights the need for further design refinements. Addressing these issues could enhance the app's clinical applicability, making it a valuable tool for bedside visual field testing and improving patient outcomes.

1. Introduction

Awake craniotomy & brain mapping

Awake craniotomy is a surgical procedure employed for the treatment of focal epilepsy and brain tumours, involving the removal of impaired cortical tissue. However, achieving a delicate balance between removing the targeted tissue with adequate margins and preserving the surrounding healthy and functional tissue poses a significant challenge. Failure to strike this balance can result in compromised cortical functions and neurological deficits. (1, 2) To address this concern, brain mapping is conducted during surgery to identify and localise specific cortical functions in the vicinity of the target tissue.(3)

Intraoperative brain mapping, frequently used during awake brain surgery, enables the identification of cortical areas responsible for specific functions through electrical stimulation. During this procedure, the cortex is exposed and subjected to electrical pulses delivered via an electrode, rendering the stimulated cortical area temporarily non-functional (4). By performing neuropsychological tests simultaneously with cortical stimulation, it becomes possible to pinpoint the precise areas within the cortex or subcortical white matter responsible for eloquent neuropsychological skills. If a patient can perform the tasks described by a specific neuropsychological test without electrical stimulation of the area related to the task but experiences difficulty performing the task during stimulation, the area associated with those skills is identified and marked. This knowledge allows the surgeon to avoid resecting functional cortical tissue, minimizing the risk of neuro(psycho)logical deficits while removing the targeted tissue with sufficient margins.

A systematic review by Ruis et al. in 2018 encompassed an extensive overview of neuropsychological tests utilized in awake brain surgery. (5) The review analysed 232 original articles, which described intraoperative measurements of single or combined cognitive domains, including language, visuospatial skills, motor/sensory functions, memory, calculation, emotion, facial recognition, musical skills, finger gnosis, and executive functions. However, most studies discussed in the review focused on monitoring linguistic skills during electrical stimulation. (5)

An unmet clinical need

Neuropsychological testing during awake surgery provides valuable insights, specifically aimed at the functional cortical areas at risk in the surgical field and facilitates the preservation of these functional

areas. However, despite careful monitoring and testing during surgery, some patients still experience neurological deficits following the surgical intervention, impeding their complete recovery. Single neuropsychological tests typically assess performance in single, isolated cognitive tasks, whereas daily activities often involve more complex functions that require engagement and interplay of multiple cognitive domains. Consequently, an unmet clinical need arises for an intraoperative testing modality capable of simulating real-life scenarios and assessing more complex tasks involving multiple cognitive domains.

Virtual reality

Virtual reality (VR) technology has gained significant popularity in recent decades. In a VR experience, users are immersed in a virtual three-dimensional (3D) environment using a virtual reality headset (VRH) or head-mounted display (HMD). Initially developed for the gaming industry, VR is now finding applications in various fields, including medical training, physical therapy, and rehabilitation. (6, 7) Given that VR experiences are presented to users through compact HMDs, they can be an interesting testing modality for the limited space available in the operating room during awake surgery. (8, 9) Utilizing VR for neuro(psycho)logical testing may facilitate more objective, standardized, and repeatable assessments, potentially reducing the impact of the researcher's experience and other interobserver variability.

Another advantage of conducting tests in a virtual environment is the ability to simulate complex real-life scenarios. This allows for the evaluation of a broader range of neuro(psycho)logical functions using only one testing modality. If this can be applied during brain mapping in awake surgery, surgeons may be able to target diseased tissue more precisely and thereby spare more functional tissue. Ultimately, this may lead to improved patient outcomes in terms of cognitive abilities, quality of life (QoL), and postoperative care.

In recent developments, eye-tracking technology has been integrated into most HMDs. This technology uses a combination of software and hardware to track and record users' eye movements as they interact with the virtual environment. (10) By collecting detailed information about users' interactions, eye-tracking technology enables further investigations into human behaviour and cognition, potentially leading to more intuitive and natural ways of interacting with virtual simulations. (11)

2. Research Objective

Ultimately, the aim of this line of research is to address the unmet clinical need in neuro(psycho)logical testing during brain mapping by leveraging virtual reality (VR) as a singular testing modality. With these means, the goal is to enhance patient outcomes by revolutionizing testing techniques in the operating room (OR) during awake surgery. As a preliminary step, this thesis focuses on one specific application of VR: the visual field assessment.

The research conducted during this graduation internship aims to lay the groundwork for future advancements in VR-based neuro(psycho)logical testing, specifically for visual field assessment, with the ultimate aspiration of refining surgical procedures and enhancing postoperative care. The goal of this thesis is to perform a proof-of-concept and feasibility study for the use of the Peili Research app, a VR kinetic perimetry application designed for the PICO Neo 2 eye virtual reality headset.

The main research question to be answered in this research is:

Is it clinically feasible to determine the visual field limits with the Peili Research app on the Pico Neo 2 eye and to identify a possible visual field defect?

To answer this question, a number of sub-questions and analyses will be explored and performed:

1. What is the test-retest reliability of this VR-based visual field assessment?
2. Will the kinetic perimetry performed with the Peili Research app generate a result similar to the Goldmann perimetry?
3. Considering the design of the application, does human reaction time affect the test results?
4. Does the colour contrast of the visual stimulus influence the resulting visual field angles?

During this internship, the foundation for semi-automatic analysis of the datasets containing the results of a visual field assessment performed with the Peili Research app will be created. The Peili app's effectiveness in detecting established visual field deficits will be explored. A manual will be developed to explain the correct use of the VRH and the Peili Research app.

3. Background

3.1 Medical Background

Human vision in short; from photon to visual field

Visual perception and the processes underlying human vision are achieved by a number of mechanisms that come together as the visual pathway. The visual pathway starts as photons enter our eye through the cornea and the lens, which collaborate to focus incoming light onto the fovea on the retina. The retina has two types of photoreceptor cells that convert the photons to neural signals. Cones, photoreceptor cells that are responsible for colour detection, have a peak density in the fovea. The other type of cells, rods, are only capable of differentiating black and white and are distributed more evenly across the retina.

Next, these neural impulses navigate through the retinal layers to the optic nerve head, where the signals converge. The signal then travels through the optic nerve fibres, via the optic chiasma and the lateral geniculate nucleus, to the cortical neurons of the visual cortex. Here, the primary visual cortex, V1, and higher visual areas process the neural signals, allowing all visual stimuli to be integrated and interpreted correctly in one coherent perception.

Preserving spatial arrangement of the visual input is an essential aspect of the human vision and, more specifically, to our stereoscopic view. Stereopsis is the ability of the brain to perceive depth and 3D spatial relationships based on the slight differences in the visual input received by each eye. (12) Using the binocular disparity created by the small distance between the eyes, our brain is able to compute and determine the distances and depths of objects in our visual field.

The visual field of a healthy individual spans around 180 to 190 degrees horizontally and 110 degrees vertically. (13) It is and consists of the monocular visual field and the binocular visual field. The monocular field is what each eye can see individually, and the binocular field is the overlapping region where both eyes' visual fields can be combined to create a single 3D perception using the principle of stereopsis. As can be seen in Figure 1, on average, each eye has a monocular field of about 135 to 150 degrees horizontally and 110 degrees vertically. The binocular field generally covers about 120-130 degrees horizontally and 110 degrees vertically.

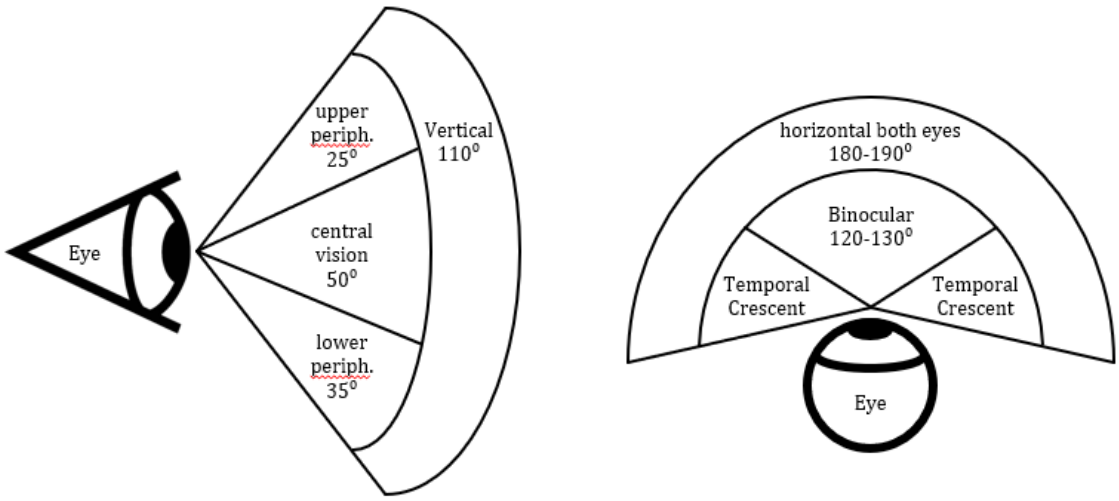

Figure 1. The visual field of a healthy individual, consisting of the monocular visual field and the binocular visual field. The image on the left (A) visualizes the vertical view, which shows 110 degrees virtually both for the monocular visual field and the binocular visual field. The image on the right (B) visualizes the horizontal visual field, which shows a binocular visual field of 120 to130 degrees next to a monocular field of 135 to 150 degrees.

Visual field defects and visual field examinations.

Visual impairment can arise from damage to various components along the visual pathway, each resulting in distinct types of deficits. (14) Clouding of the lens, as seen in cataracts, can lead to decreased light sensitivity, where damage to the retina caused by macular degeneration can cause central vision deficits. Figure 2 illustrates how the location of a lesion along the visual pathway can be deducted from the presented visual field deficit. (13) Defects anterior to the optic chiasm will lead to unilateral visual field impairment, while homonymous deficits indicate that the lesion will be located further along the visual pathway, contralateral and posterior to the chiasm.

Deficits to the visual field can be identified and quantified by performing standardized and objective visual field assessments. The current standard method for evaluating the visual field is perimetry. In general, two types of perimetry can be distinguished: static perimetry and kinetic perimetry. (15)

Static perimetry primarily aims to determine areas in the visual field with a reduced sensitivity. Here, the patient is asked to gaze to a focus point while light stimuli with different sizes and intensities are presented in various areas of their visual field. The patient is asked to indicate whether they can perceive the stimuli, allowing the researcher to determine areas with reduced sensitivity and quantify these deficits. While static perimetry is able to investigate the limits of the visual field, this test's main objective is to assess the central visual field, typically the central 30 degrees. (16, 17) Kinetic perimetry extends its evaluation more often to both central and peripheral areas and is more sensitive towards edge detection of defects.

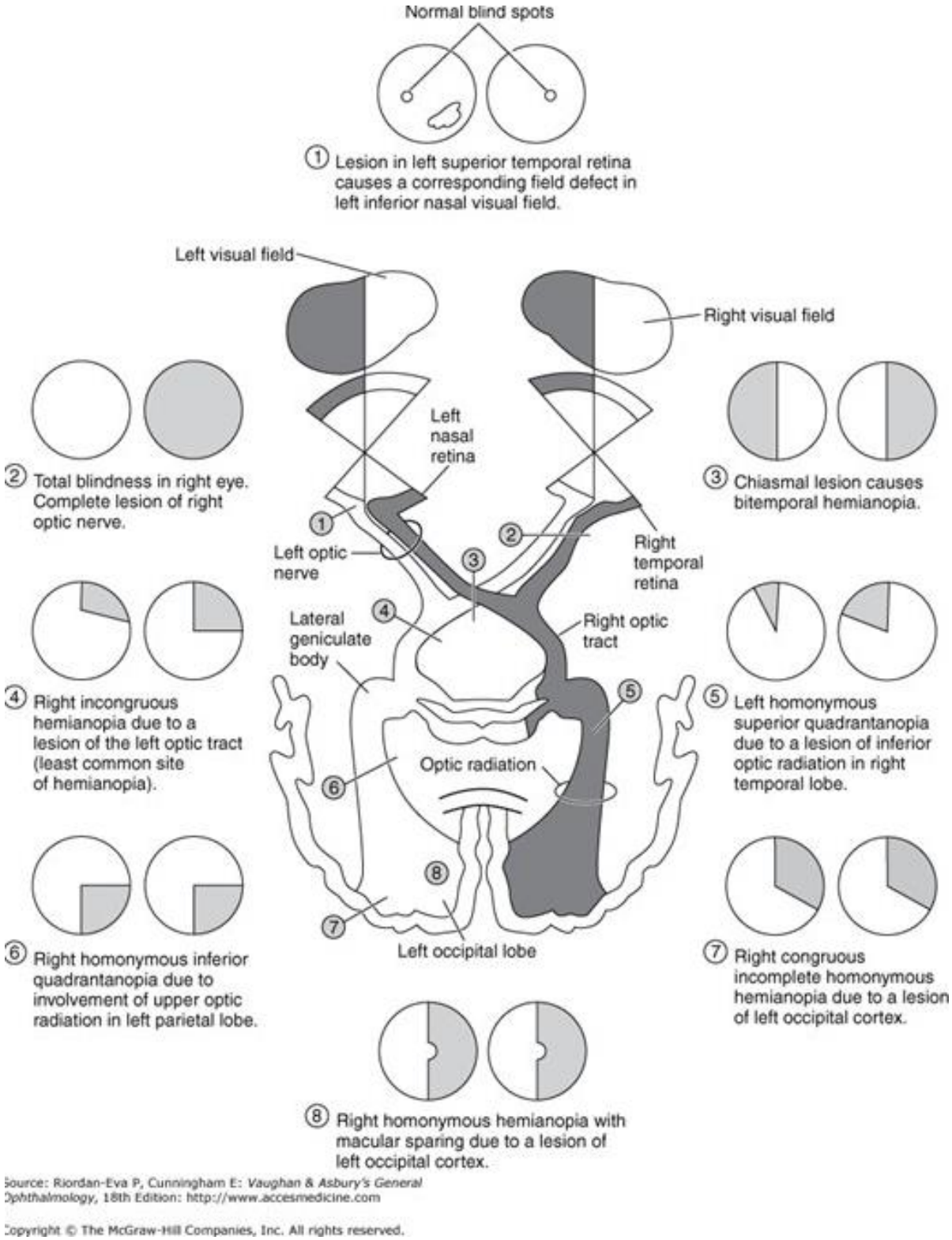

Figure 2. Visual field defects caused by lesions on different locations along the visual pathway (13). Lesions to the optic nerve or the retina can be recognized by unilateral visual field loss. Damage to the optic chiasm is characterized by bitemporal hemianopsia. If the visual field is compromised on the same side of both eyes, known as contralateral homonymous visual field defects, this is generally caused by lesions posterior to the chiasm.

Kinetic perimetry, or Goldmann perimetry, focusses on determining the boundaries of one's visual field. (18-20) During this assessment, the patient is asked to maintain their gaze on a central point while a visual stimulus moves from the periphery towards the centre of the visual field. The patient responds when the stimulus enters their visual field. It is recommended that the speed of the stimulus is standardized at 2-4 degrees per second to optimize the correct identification of visual field limits. This minimizes effects due to human reaction time but does allow the velocity to be significant enough to be detected with kinetic sensitivity. (21-23) By systematically executing this test with the stimulus entering the field from different angles, the boundaries of the patient's visual field can then be identified and plotted in arc degrees. The graph that represents these boundaries is called the isopter. Key aspects influencing the arc degrees of the isopter are luminance contrast, colour contrast, and size of the stimulus. (24, 25) Through reiterating the examination with varying object sizes or luminance intensity levels, a range of isopters can be created for an individual eye. (26) Object sizes in Goldmann perimetry range from 1/16 mm^2 (size I) to 64 mm^2 (size V), with stimulus brightness indicated by a combination of numbers and letters (e.g., 4e). The 4e setting represents maximum brightness and least attenuation, corresponding to approximately 0 dB, with each step down in brightness (e.g., 3e) adding roughly 10 dB. Figure 3 shows the positions of isopters for different stimulus sizes and luminance levels. (27) The figure provides a visual comparison of the normal isopters obtained using different Goldmann perimetry stimuli. It shows that the visual field extents vary with changes in stimulus size and brightness, with the largest field observed for the V4e stimulus and progressively smaller fields for III4e, I4e, and I3e stimuli. This illustrates the effect of stimulus properties on the mapping of the visual field in normal vision.

While testing various luminance contrasts and stimulus sizes are indicated in Goldmann perimetry, colour contrast is not often used. The ability to detect colours and colour contrast between stimulus and background varies between individuals. However, it sometimes may have the same effect as varying luminance contrast, suggesting that it would be impractical and occasionally redundant to test both for investigating visual field limits. (24, 28)

While Goldmann perimetry is widely considered to be the gold standard for assessment of the peripheral visual field, it is also accompanied by a few limitations. An important limitation reported in scientific literature is that the test must be conducted by a trained clinician or perimetrist. As the test is performed manually, the perimetrist has influence on the velocity with which the stimulus is presented, which makes the test prone to interobserver variability. (16, 29, 30)

Besides limits to the execution of the test and the standardization of the results, Goldmann perimetry has another limitation. Due to the size of the Goldmann Perimeter, the test can only be performed on mobile and cooperative patients. As the perimeter is large and heavy, it cannot be moved around easily, and it is impractical for bed-side use.

Similarly, with limited space available in the OR, a full visual field analysis such as a Goldmann perimetry is not possible. As an alternative, a simpler confrontation visual field assessment is preferred during electrical cortical stimulation, to obtain a rough indication of the boundaries of the patient's visual field.

In an (outpatient) clinical setting a physician can perform the confrontation visual field to screen for visual field defects. (31) During the confrontation visual field test, each eye is assessed separately. The physician is positioned opposite to the patient while the latter is asked to focus on the examiner's nose. This ensures that the patient's gaze remains steady throughout the examination. The physician presents

a number with his fingers within the central visual field, asking the patient to indicate how many fingers he is holding up. The peripheral visual fields are tested in a similar way, but now the physician moves their fingers in each of the four quadrants. The examiner holds their hands apart and simultaneously flashes fingers in both the nasal and temporal hemifields. The same is done above and below the horizontal meridian to test the upper and lower portions of the visual field. Any discrepancies in the patient's responses may indicate visual field defects in the corresponding eye(s).

While the confrontation test can provide an indication of visual field defects in bedside settings or during awake brain surgery, solid and accurate quantification of the outer limits of the visual field cannot be determined this way.

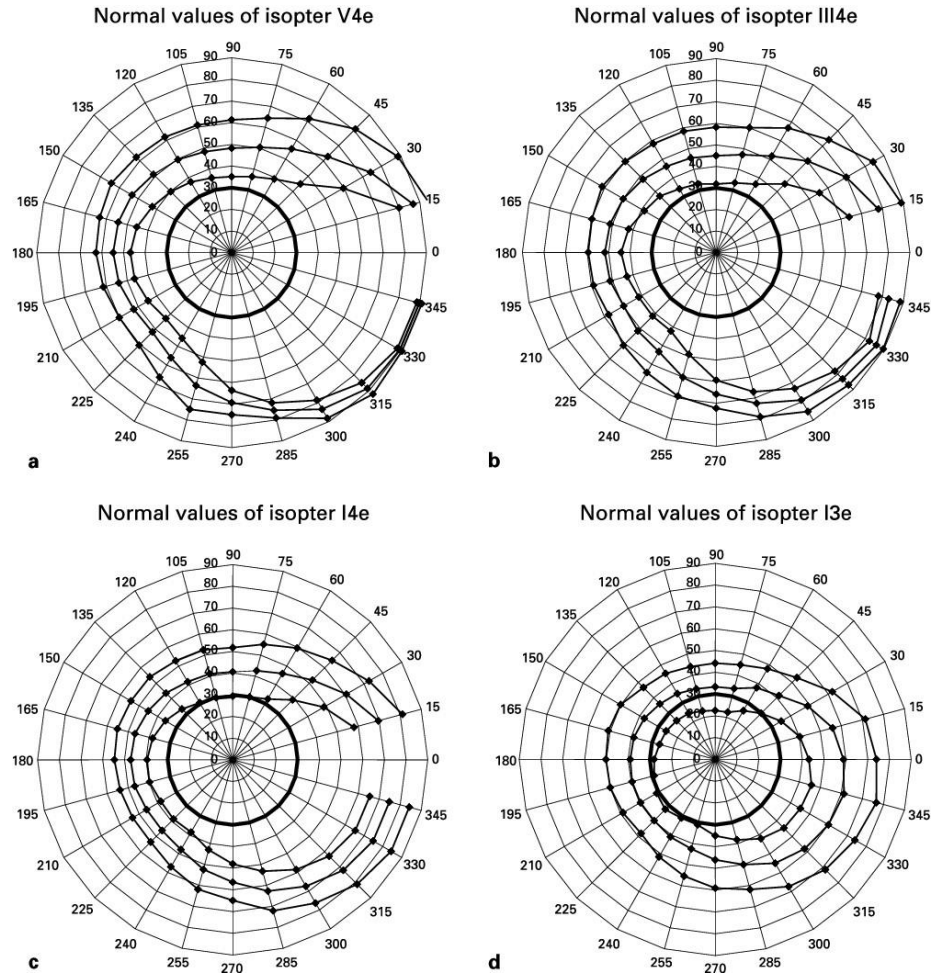

Figure 3. Normal positions of isopters for healthy individuals aged between 19 and 42 years. Figure (a) shows the isopter for the largest and brightest stimulus (V4e), while figure (b) displays the isopter for a medium-sized, bright stimulus (III4e). Figure (c) represents the isopter for a smaller, moderately bright stimulus (I4e), and figure (d) shows the isopter for a similar size stimulus with slightly reduced brightness (I3e). These isopters demonstrate the typical visual field extents for each stimulus condition under normal vision. Each figure shows the average positions of the isopter ± 2 standard deviations.

3.2 Technical Background

Virtual reality and Eye-tracking

In VR, the immersive 3D environment is created by using stereoscopic 3D technology. This simulates the way human vision perceives depth and is established by offering each eye a separate image, that represent the same scene, but from a slightly different angle. These disparities mimic the small distance between the human eyes, and through combining the perspectives from the left and right retina, a sense of depth is created by the visual cortex. (32)

In the most recently designed VRHs, eye-tracking technology is integrated with the device. In general, eye-tracking is accomplished using a combination of light reflection and of refraction, which is the principle that light waves change directions when passing from one medium to another (33). The system uses infrared light, which is not visible to the human eye and does not interfere with vision, directed at the user's eye. This light is then reflected differently by the various structures of the eye and these reflections are detected by an infrared sensor. Based on the patterns of these reflections and any changes in positions of reflections, the direction of the user's gaze can be estimated.

To correctly establish the relationship between the detected reflections and the actual gaze direction, it is essential to calibrate the eye-tracker for each individual. By calibrating and validating the eye-tracker, interpersonal anatomical variations can be minimised, thereby improving the accuracy of the resulting eye-tracking data.

In VRHs, eye-tracking calibration is often performed in three steps: data collection, optimization and validation. During the first step, data collection, the user is instructed to focus on a sequence of predefined targets on the screen. The calibration targets can range from 2 targets, 5 targets or 9 targets. Next, the eye-tracker is optimized. This is done by comparing the reflection and refraction data that was collected in the previous step with a standard 3D eye model. The standard model is optimized and able to map the gaze data to screen coordinates more accurately. Finally, the resulting personalised 3D eye model is validated by offering a set of validation targets and using the obtained data to calculate the average error.

A single eye tracking datapoint represents the gaze of the user at a timepoint. The gaze of the user is defined as the combined gaze of both the left eye and the right eye. The gaze ray vector is generally represented by an origin and direction. The origin indicates the origin point and the direction is a normalized vector indicating the direction of the gaze ray. The units are in millimetre (mm). As shown in Figure 4A & B. The image on the left (A) visualizes right hand sided the eye-tracking coordinate system. The image on the right (B) visualizes left hand sided coordinate system used by most virtual reality headsets to indicate their location in world space.eye tracking data use a native right hand coordinate system, but the data is often saved after the engine performs transformation to the "local space" cartesian coordinate system or the "world space" cartesian coordinate system. Both the local and world space use left hand sided coordinate systems, as visualized in Figure 4B.

In the local coordinate system, the origin is shared with the VR camera. An advantage of this system is that the reported eye tracking data is invariant to head movements. Generally, the world space is used as the primary tracking coordinate system as the objects in the virtual scene then share the same tracking space. The alignment of these coordinate spaces requires the integration of the eye-tracking data with the location and direction of the headset.

There are two primary methods for transforming real-time eye-tracking data into world space coordinates: the first involves using historical head pose data corresponding to the time when the eye-tracking data was captured. This method tends to be the most accurate, as it closely aligns the eye-tracking data with the head's position at the precise moment of data capture. However, this approach can introduce latency, as the system must wait for the appropriate head pose data to be available before rendering the visual environment. This latency, although small, can lead to VR motion sickness, especially during rapid head movements or when precise visual synchronization is required for the experience. (34)

The second method uses the head position predicted from the previous movements to transform eye-tracking data into world coordinates. This approach reduces the lag, providing a more immediate visual response. However, it is less accurate during quick, unpredictable head movements, potentially leading to misaligned visualizations and a less immersive experience. The choice between these methods depends largely on the specific requirements of the VR application—whether it prioritizes real-time responsiveness or precise visual alignment. (34)

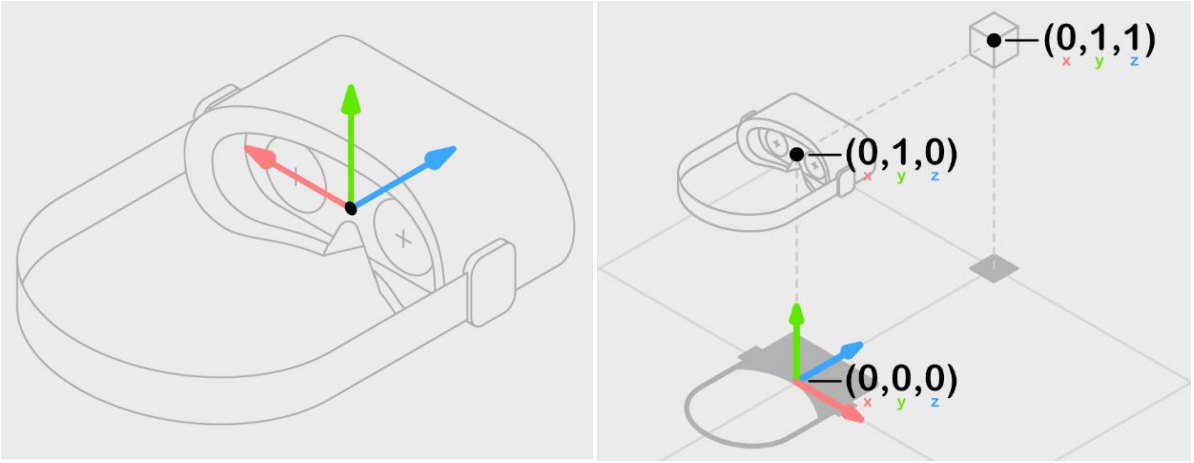

Figure 4A & B. The image on the left (A) visualizes right hand sided the eye-tracking coordinate system. The image on the right (B) visualizes left hand sided coordinate system used by most virtual reality headsets to indicate their location in world space. (34)

Technical challenges in VR

A high-quality virtual reality experience is characterized by a high level of immersiveness. This realism is created by optimizing the added value of the different technologies and overcoming some of the challenges accompanying them. Three essential pillars contribute to the immersive experience: low system latency, high-resolution displays and a wide field of view (35-37).

System latency, defined as the delay between a user's action and the corresponding response within the virtual environment, is a fundamental factor in maintaining immersion. Higher system latency is closely associated with the onset of virtual reality sickness. (38) VR sickness is defined as a sensory conflict between visual and vestibular inputs as a result of the use of VR technology.(39) Symptoms include

nausea, dizziness, and disorientation. (40, 41) Minimizing system latency is, therefore, essential to reducing the risk of VR sickness and enhancing user comfort in VR environments. To achieve low latency, many VR headsets use predictive algorithms that generate forward projections based on historical data. This enables the system to anticipate user movements and adjust the visual environment accordingly. The perception of lag is minimized this way, which is crucial for preventing cyber sickness and maintaining a coherent experience. In addition to the predictive algorithm, the use of higher refresh rates can further reduce the perceived latency by enabling smoother transitions between frames.

The other two pillars of an immersive VR experience are the resolution of the displays and the FOV of the used VRH. (36) High-resolution displays contribute significantly to creating a detailed and realistic environment. (36, 42) However, the demand for high resolution must be balanced with the system's overall performance to prevent overloading the hardware, which can lead to reduced refresh rates and increased latency. This balancing act is further complicated by the need to support a wide FOV, which is often limited by the physical and optical constraints of current VR headsets.

As mentioned earlier, the FOV of a healthy individual spans around 190 degrees horizontally and 130 degrees vertically. (43) In contrast, VRHs generally do not exceed 100 degrees horizontally. This discrepancy means that most head-mounted displays (HMD) fall short of matching the total human visual field.

Furthermore, research conducted by Sauer et al showed that the field of view advertised by a number of manufacturers is significantly different from the field of view in practice. (44) They researched the influence of mean eye relief distance on the experienced field of view. Mean eye relief distance was defined as the distance from the VRH lens to the user's eye lens. This distance was found to significantly reduce the effective FOV experienced by the user. For example, while the Pico Neo 2 headset is advertised with a 101-degree FOV, it effectively provides a binocular vertical and maximum horizontal field of view of around 88 degrees. (44)

The trade-off between processing power and the three pillars remains challenging in VR. Integrating these three determinants of an immersive experience into a device requires a high amount of computational power from the headset. While the hardware capable of this processing power does exist, adding it to the VRH would be impractical due to the increase in weight, size and heat generated by the headset. This would decrease user comfort. Additionally, the extra weight can make it difficult to properly fixate a VRH that is too heavy, which could result in a small shift over time, compelling the user to reposition the headset. For headsets that have integrated eye-tracking technology, this may also lead to inaccuracies in the eye-tracking data. In order to optimize the experience whilst minimizing the computational power required, a technique called foveated rendering is often used in VRH.

Foveated rendering is a technique often used in VRH to lower the processing and computing requirements of visualising a 3D environment. (45) In foveated rendering, the area where the user's gaze is focussed on is rendered in a higher quality and the surrounding areas, in the user's periphery is visualised with a lower resolution and with fewer details. Two types of this technique can be distinguished: static foveated rendering and dynamic foveated rendering. In static foveated rendering the centre of the screen is always shown with the highest resolution, and the resolution gradually decreases towards the peripheral areas. Dynamic foveated rendering is only possible in VRH with integrated eye-tracking. Here, the device determines the direction of the user's gaze based on the eye

tracking data. This data is then used to determine which area of the display has to be rendered with a higher resolution. The surrounding or peripheral area, that does not have the users focus, is then rendered in a lower resolution. By lowering the resolution in some areas, processing capacity is freed up that can be used to improve the refresh rate of the VRH, which allows for a smoother experience.(46)

In addition to specific challenges with (head-mounted) VR devices, this technology also faces several general challenges encountered by all electronic devices. Sensor noise can introduce random variations, and environmental interference, such as electromagnetic noise or user movements, can disrupt the system. Sensor drift, particularly in devices using accelerometers, can cause the perceived orientation and position to become inaccurate over time.

While eye-tracking in virtual reality headset is accompanied by number of challenges, it also introduces the possibility of generating and deducing a broader range of variables that can be analysed during visual field assessments. These variables should be explored for their (potential) added value and prioritized accordingly. The following section explores previous work on visual field assessments using VRH, to determine potential metrics of interest. In addition, previously conducted research can be used to identify and prevent earlier mistakes, thereby improving the methodology.

3.3 Previous work on visual field assessments using VR

Over the past 25 years, performing visual field assessments with virtual reality has increasingly been investigated. This increase in research can be attributed to a growing recognition of the potential of VR as a low-cost perimetry modality. As many articles describe the capability of performing objective bedside visual field assessments as an important incentive for their research, the growing number of publications can be interpreted as an indicator of the efforts for meeting this clinical need.(47)

Various combinations of software packages, VR applications and VR devices have been investigated. (16) Generally, most studies show that performing perimetry yields comparable results to perimetry performed using standard automated perimetry. (48-52) For example, research conducted by Narang et al. compared their visual field assessment with the standard for static automated perimetry, the Humfrey Field Analyzer. (53) Their research found a high corelation between the two tests, with an intraclass correlation coefficient of 0.893 ($P<0.001$). In 2023, Selvan et al. performed a systematic review of 64 studies with the aim to investigate the use of virtual reality headsets for perimetry testing. (54) From their research. they concluded that VRH perimetry performance is similar or maybe even superior to standard automated perimetry.

However, it must be noted that almost all publications have performed assessments of the central visual field as opposed to the peripheral limits of a visual field. Most articles reported on conducting static perimetry and standard automated perimetry for the central 48 degrees (24-2) or 60 degrees (30-2). As stated earlier, VRHs often provide a smaller FOV compared to the human visual field. Consequently, the angle that can be tested using a VRH may not be sufficiently large to determine the outermost boundaries of the visual field. A larger FOV is necessary for accurately assessing the full extent of the peripheral visual field, which might limit the effectiveness of VRHs in such evaluations.

To date, there is one previous study that has performed kinetic visual field assessments using a VRH. In 2023, Terraciano et al. published the results of their portable automatic kinetic perimeter on the Oculus Quest 2 in comparison with the Humphrey Field Analyzer 3 perimeter on healthy participants. (16) In

the virtual environment of their kinetic perimeter, a Goldmann bowl with a 30 cm radius was constructed, and stimuli were presented by moving radially from the bowl's periphery towards its centre along predefined vectors. A fixation point was placed at the centre of the bowl, and participants were instructed to maintain their gaze upon this focus point. The researchers used target luminance and size corresponding to the standards of Goldmann kinetic perimetry. The visual stimuli approached the centre of the bowl at a constant angular speed of 5 degrees per second. The visual field assessments were performed under binocular vision conditions, though measurements were taken for each eye individually. This was achieved by presenting the stimulus on one of the two displays of the VRH. For example, when testing the right eye, the target was displayed solely in the right visual display.

The results from the Oculus-based kinetic perimetry were largely comparable to those of the gold standard, though minor differences were noted. Specifically, the gap between the sizes of different isopters was smaller in the Oculus perimetry than in the Humphrey perimetry, which the researchers attributed to potential effects related to the patient's focus and the stimulus's light intensity. Interestingly, despite concerns about the limited FOV of VRHs, this study demonstrated that a sufficiently large angle could be assessed using the Oculus device, suggesting potential for VRHs in kinetic perimetry.

4. Methods

4.1 Data acquisition

This feasibility study was conducted in cooperation with the Department of Neurosurgery at the Amsterdam University Medical Center (AUMC).

The application used for the visual field assessment was created by Peili Research. The app runs on the Pico Neo 2 eye VRH. The data extracted for this research is a combination from app data and eye-tracking data from the VRH.

For the VRH to be used during this research, the Pico Neo 2 Eye, stereopsis is achieved by offering each eye a different image on the single LCD display with a 4K (3840x2160 pixels) resolution that operates at a refresh rate of 75 Hz. The headset uses foveated rendering and has a reported field of view (FOV) of 101 degrees. The eye-tracking technology that is integrated in the Pico Neo 2 eye uses standard 5-point calibration. Gaze data output is generated at a frequency of 90Hz and includes (combined) gaze origin and direction. It has an ideal eye rotation accuracy of 0.5 degrees.

In addition to performing the kinetic perimetry with the VRH, an official Goldmann perimetry was conducted.

4.2 VR Peili Research set-up

Volunteers partaking in the study are asked to use the Pico Neo 2 Eye that is running the Peili Research VRH application. Simultaneously, the researcher operates a Samsung tablet running the corresponding Peili Research application designed for the tablet. The connection between the VRH and tablet is established through WiFi. A step-by-step guide of how the test was performed can be found in Appendix B: Manual for Peili app.

Before the visual field assessment, the eye-tracking technology is calibrated through a standardized 5-point calibration, where the volunteers are instructed to follow a dot's trajectory over five points with their gaze. The process is reiterated for validation of the calibration results. After the eye-tracking calibration and validation, the researcher initiates the visual field assessment through the tablet interface.

During the assessment, participants are asked to fixate their gaze upon an off-centred black focus point projected on a grid. Participants are explicitly instructed to focus on this point throughout its observable duration. After one full second of correctly gazing at the focus point, a dot appears at the opposite side from the off-centred focus point and follows a linear trajectory directly to the focus point.

The use of an off-centred focus point is crucial in this procedure. The idea behind this is that the Field of View (FOV) of the VR headset (reported as 101 degrees by Pico and averaged at 88 degrees by Sauer et al.) is smaller than the human FOV, which is 180 degrees. By using an off-centred focus point, the effective angle that can be tested with the VR headset is increased, allowing for the assessment of the extreme peripheral angles of the human visual field.

The volunteers verbally indicate the moment at which the dot enters their visual field, whilst gazing at the focus point. The researcher logs this through the app's interface on the tablet. In addition to providing verbal confirmation, the volunteer is also requested to press a button on the Pico controller as the dot enters their visual field. The dot continues the linear trajectory to the focus point until it reaches the focus point. Then, the next dot appears and follows a linear trajectory at a 45-degree angle from the first trajectory, and the process is repeated. For each focus point, a sequence of three dots appears. The first dot is always blue, the second dot is always green, and the third dot is always yellow, and the background is always a blue sky with clouds behind a black grid. Figure 5 shows a visualisation of what the volunteer is shown in the Peili environment on the VRH.

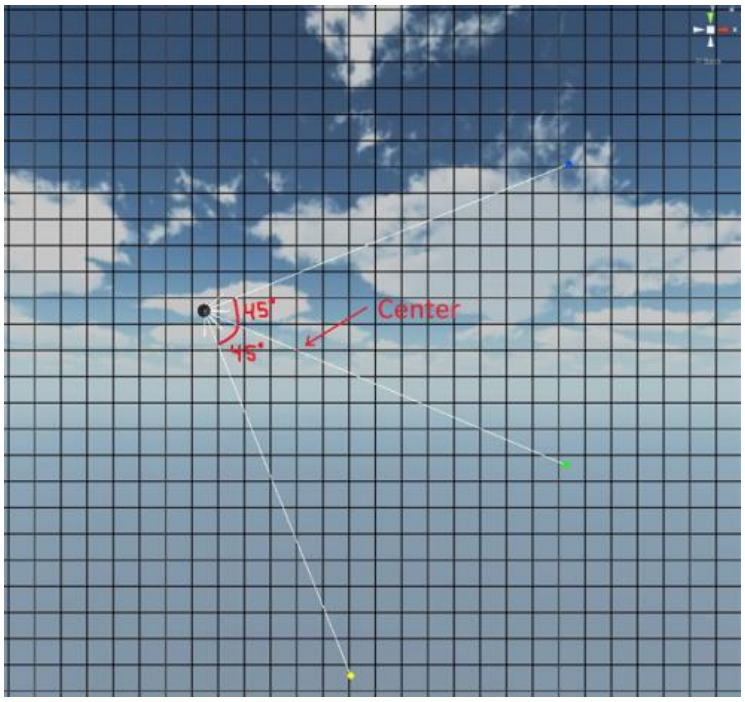

Figure 5. Visualisation of the virtual testing environment in the Peili app run on the PICO Neo 2 eye. The black dot visualised is the off-centred focus point where the participant is asked to focus their gaze on. The smaller blue, green and yellow dot will enter the screen consecutively, and will follow their respective trajectories until they reach the black focus point. The three dots enter the screen at a 45 angle with each other.

This approach is repeated in a systematic way for focal points spread out in a quadrant layout. After the assessments in all quadrants have been performed, the researcher saves the data on the VRH through the tablet's app interface, and the test is completed.

The data set can be extracted from the VRH by connecting the headset with a computer through a USB connection.

4.3 Data description

The extracted data set contains 1 Text document that is named "Results" and 5 JSON files named "DataRecords", "EventData", "EyeTrackingData", "EyeTrackingValiationResult", and "TrackingData". No supplementary documentation providing clarification on the data sets is included.

The text document, "Results", is a summary of the found results, including total recording time, number of controller clicks, the time stamps at which the dots were confirmed to be visible. In addition, the total movement, speed and rotation, both for the controller and for the head movements are reported.

The "DataRecords" file contains a summary of results as are stated in the "Results" text document, but in a JSON format. This JSON file also specifies which found results are included to the overview in "Results" file; the default assumes that every result in this file is exported to the text file.

The "EyeTrackingValidationResult" file features the results of the calibration and validation of the eye-tracking technology, such as the locations of the validation points, the average gaze delta, the average gaze standard deviation, and the final score.

In the "EyeTrackingData" file, the local gaze ray and the world gaze ray coordinates are saved from the start of the recording until the end of the exercise. For every eye-tracking data point stored here, a number of other metrics are saved including the time since startup, whether the left and right are closed, and if the saved data is valid. The unit used for eye-tracking coordinates is meters (m).

"TrackingData" holds information on the movements and activity of the VRH at timepoints also defined as the time since the startup. Metrics saved in this data set include the position, rotation, scale, velocity, and angular velocity of the VR Camera. In addition, data regarding the movements of the dots used in the visual field assessment of the Peili Research app, are also defined as the position, rotation, scale, velocity, and angular velocity.

The "EventData" JSON file comprises all data on changes in recorded variables and app settings during the visual field assessment. The various events that are documented in this file include:

- Coordinates of (current) focus point position relative to camera
- Coordinates of gaze hit points, the gaze over
- Coordinates of last gaze hit points, the gaze out
- Indications of changes in focus point request
- Focus Success time indications
- Indications of button clicks on the controller
- Confirmation of visibility of the dots by the researcher
- Resolved focus points

All events included in the "EventData" file are accompanied by two timestamps: one timestamp as defined by the Peili app, "time", and one timestamp defined by the VRH, "TimeStamp". The Peili time starts running as the visual field assessment is initiated, and the VRH time starts counting from the moment the Peili App starts with validation of the eye-tracking technology. This last time indication is also used across the other JSON files.

4.4 Data analysis

Data analysis is performed using MATLAB 2023b (MATHWORKS Inc.) The script designed for this thesis has the following general structure:

- Main script looping over each dataset:
    - Load JSON files
    - Preprocessing
    - Extract and structure the required data
    - Check for incorrect identification of dots
    - Transform coordinate system
        - Translate
        - Rotate
        - Cartesian to polar
    - Comparing different visual field estimations
    - Save all processed and structured patient data
- Analysis 1 - Repeatability: comparing 10 visual field results from 1 participant
- Analysis 2 – Comparison with Goldmann visual field results
- Analysis 3 – Human reaction time
- Analysis 4 – Effect of dot colour contrast

Main script

Loading JSON Files: First, the raw data was stored in separate arrays. Due to the difference in coordinate systems used by VR and MATLAB, specifically right-handed versus left-handed systems, it was essential to reverse the z-axis during data import. This adjustment ensured that positive values were converted to negative and vice versa. For all analyses, the coordinates in world space were used.

Preprocessing: The eye-tracking software automatically identifies valid and invalid data points based on the presence of reflections. For example, data collected during a blink will be labelled as invalid since no infrared light reflection was detected, but it is still saved. The raw data, therefore, still contained invalid data. Merely removing invalid data points, however, would be insufficient as the movement, both preceding and following the closure of the eye, will also influence the data. To address this, a buffer period corresponding to the duration of a blink was implemented around the invalid data points. As described by Navascues-Cornago et al, the average duration of a blink is around 0.1 seconds, during which closing the eye takes longer than opening the eye. (55) Therefore, invalid data points were removed, with a pre-blink buffer larger than the post-blink buffer. Next, the data was filtered using a 45 Hz low-pass filter to eliminate any high-frequency noise. (56, 57)

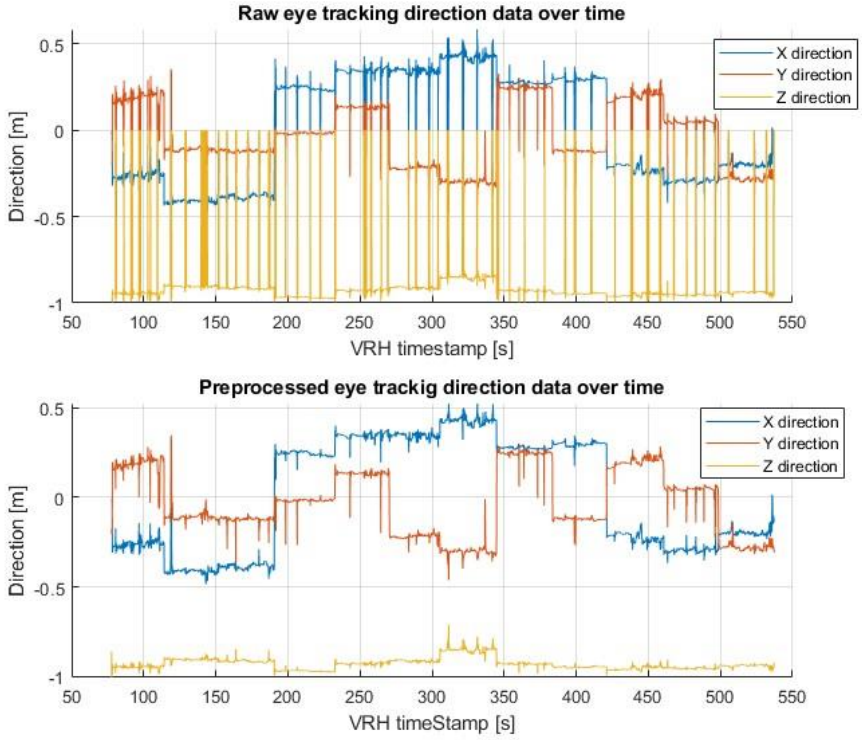

Figure 6. Visualisation of eye-tracking direction in world coordinates over the time of the virtual reality headset. The top figure, figure A, shows the raw eye-tracking direction data before preprocessing. The figure below, figure B, shows the eye-tracking direction data after removal of the blinks and applying a low pass filter.

Structuring data: All data were systematically organized according to each focus point. This was accomplished by utilizing focus point-resolved timestamps, which indicated when there was a transition between displayed focus points, allowing the determination of start and end times for each focus period. Additionally, the focus point-resolved variable included timestamps recorded by the researcher on a tablet, marking when the participant acknowledged the appearance of a dot in their visual field. These tablet confirmation timestamps were stored for each focus point. During the assessments, the participant was instructed to press a button on the controller as the dot entered their visual field. The timestamps of these button presses are stored as 'dot confirm controller'.

During the visibility period of the focus points, three dots moved consecutively. It was predetermined in the app software that each dot took 10 seconds to reach the focus point along its path. By differentiating their positions, indicated by Cartesian coordinates, it was possible to determine the timeframes during which the dots approached the focus point. The 10-second time window containing the largest values for the differentiated positions is used as the window of movement for each dot.

By analysing the intervals during which the dots moved, the dot confirmation timestamps could be linked to the respective dot numbers. However, occasionally a dot has been misclassified, and has not been confirmed or confirmed double during the movement interval of a single dot. For example, there could

be four dot confirmations within a single focus point interval, despite only three dots entering the visual field.

Corrections for such anomalies were made based on several rules. For each focus point identified as having unexpected results, such as missing dot stamps or duplicates, the original dot confirmations were stored in a separate structure for reference.

First, for focus points with more than three dot confirmations present and no missing labels or unlabelled confirmations, the dots containing duplicate confirmations were removed to ensure that unique confirmations were retained.

Next, the focus points that had three or fewer confirmation timestamps were addressed. For focus points that missed confirmation timestamps, the function assigned appropriate dot labels and positions based on the available data. This ensured that each of the three expected dots (dot1, dot2, dot3) had a corresponding timestamp and position, filling in any gaps in the data. Duplicate confirmations were systematically addressed by reassigning labels where necessary. The function checked for and corrected duplicates sequentially for each dot (dot3, dot2, and dot1). If a duplicate was found, the timestamp and position of one of the duplicates were reassigned to the next available dot, ensuring that all dots had unique confirmations. If reassignment was not possible, the duplicate labels were removed to prevent data from being included in the analysis. The function performed a final check to ensure that the number of unique dot labels coincided with the number of dot confirmations.

Transforming coordinates: The coordinate system was transformed to position the VRH at (0,0,0), facilitating the calculation of visual field angles. While focus point positions relative to camera were provided in the event data set, these positions were not used. From exploratory plots, it was found that these positions relative to camera did not visualise the focus point correctly with respect to the other elements in the virtual environment. Therefore, the location of the focus point was determined by averaging the endpoints of the three dots. Following this, all coordinates were translated with respect to the world origin and then rotated based on the translated coordinates of the focus point.

Next, the Cartesian coordinates were converted into polar coordinates to represent the angles of the isopter. This conversion was performed using *Equation 1*, corresponding to the method outlined by Sauer et al. (44) in their study. In the equation, φ represents the polar angle or the azimuth radians. This can be seen as a representation of the two-dimensional cartesian coordinates as the angle of the meridian through the origin (the centre of the visual field). The theta angle θ, or elevation, represents the field of view limits in this direction in radians.

$$\begin{pmatrix} \varphi \\ \theta \end{pmatrix} = \begin{pmatrix} arctan\,\frac{x_\omega}{y_\omega} \\ arctan\,\frac{\sqrt{{x_\omega}^2 + {y_\omega}^2}}{z_\omega} \end{pmatrix}$$

Equation 1. Calculation for the conversion of the Cartesian coordinates to polar coordinates. In this equation, φ represents the polar angle ranging from 0 to 360 degrees and θ represents the angle from the centre of the visual field. The x_w, y_w, and z_w represent the respective coordinates in the Pico Neo 2 eye's world space. (44)

Saving data for analysis: At the end of the main loop, the structures containing the relevant data for each focus point were saved for further analyses.

Analysis 1: Test-retest reliability

The 10 obtained datasets were used to assess the test-retest reliability and variability of visual field examination performed with the Peili Research app on the Pico Neo 2 eye.

First, linear interpolation was performed to handle any missing data points in the dataset. The interpolation standardised the length of the data vectors across tests, which was required for subsequent analysis. Exploratory scatter plots were created to visually inspect the distribution of θ and φ values across all tests. The coefficient of variation was determined for each data set. Next, the Shapiro-Wilk test was used to determine for each dataset if the visual field angles had a normal distribution. Levene's test for homogeneity of variances was performed to assess the homogeneity of variances.

Based on that result, the function computed either Pearson or Spearman correlation matrices to examine the linear relationships between the found angle values from different tests. Pearson correlation were to be applied if the data met the requirements of normal distribution and homegneity of variance, otherwise the Spearman correlation would be applied. Additionally, the Intraclass Correlation Coefficient (ICC) was calculated to assess the reliability of measurements across tests, providing an indicative measure of consistency.

Analysis 2: Comparison with Goldmann perimetry

In order to compare the visual field obtained through the Peili Research app and the Goldmann perimeter, both visual fields were visualized in isopters. The results of the Goldmann perimetry were provided on paper and were only available in hardcopy. The comparison of the results of the visual field assessments was conducted through visual inspection of their isopters.

To assess the feasibility of using the Peili app to test the visual field, it is essential to determine the maximum visual angle that can be tested. An effective visual field test ideally covers up to 180 degrees. However, the field of view (FOV) of the Pico Neo 2 Eye headset is reported to be 101 degrees under optimal conditions by the manufacturer, while Sauer et al. found it to be approximately 88 degrees on average. (44)

The app was designed to increase the testable angle by projecting off-centred focus points. When participants focus on these off-centred points, and the stimulus enters from the opposite side of the visual field, the effective angle being is increased. This method allows the app to measure a larger portion of the visual field, potentially reaching the maximum visual angle for a user.

To determine if the angle was increased sufficiently an analysis was performed to determine the angle of the focus points to the centre, thereby quantifying the increase in the effective angles tested throughout the assessment. The mean angle of the focus point to the centre, the lowest tested angle, and the maximal tested angle were calculated across all focus points.

Analysis 3: Human Reaction Time

The Peili Research app is designed so that the participant verbally confirms when a dot approaches their visual field. The researcher then records this timestamp by pressing a button on the tablet. It was hypothesized that the noting down of confirmations by the researcher on the tablet may lead to misleading visual field limits due to human reaction time. As the Peili application has hardcoded the dots to approach a focus point at a constant speed and in 10 seconds, the time it takes the researcher to process a verbalized confirmation and record it in the app could lead to results showing significantly

smaller visual field limits. Therefore, during this study, the participant was asked to simultaneously push a button on the controller when an approaching dot entered their visual field. The timestamps of the confirmation through the tablet and the confirmation through the controller were compared to determine the potential impact of the human reaction time on the visual field limit results. The mean, standard deviation and confidence interval for the time and angle differences between tablet and controller confirmations were calculated.

Statistical analysis was performed by conducting a paired t-test on the confirmation timestamps of the tablet and the controller. Another paired t-test was performed on the angle of the dot with the gaze direction on those confirmation timestamps. The null hypothesis for both tests was that the confirmation method did not influence the results. The paired t-test results included p-values to indicate the likelihood that any observed differences were due to chance, and a hypothesis test result indicating whether the null hypothesis (no difference) could be rejected.

Analysis 4: Colour contrast of the dots

During the visual field assessment performed with the Peili app, the three dots approaching each focus point consecutively are visualised in different colours (see Figure 5). As described in chapter 3.1 Medical Background, research has shown that variations in colour contrast show similar effects as variances in luminance contrast when performing visual field assessments. This raised the question if the differences in colour contrast among the approaching dots influenced the visual field angle at which each dot's presence was confirmed in the current test set-up. To investigate this, the visual field angles at the time of dot confirmation were categorized into three groups based on the colour of the dots: blue, green, and yellow. The data was plotted by colour on a polar plot to facilitate an exploratory visual inspection of the distribution of dot confirmations.

For each colour, the mean visual field angles and the standard deviations were calculated. The non-parametric Friedman test was used to identify if there were significant differences in the visual field angles found for each dot colour. If the Friedman test confirmed that there were significant differences between the angles, post hoc analysis was performed with an adjusted significance level ($p<0.01$) to account for multiple comparisons.

Analysis 5: Clinical application and calibration quality

While this research was being performed, an opportunity arose to collect data from volunteers in the neurosurgery department. This made it possible to perform some preliminary tests and to explore if the use of the Peili app on the Pico Neo 2 eye was clinically feasible in its current form. Thereby, investigating if any practical limitations may arise when performing the test bedside on post-op volunteers.

These volunteers had known visual field defects and had recently undergone brain surgery. It was explained to the volunteers that this research was still in its early stages and had not yet received official approval. They were instructed to remove the VR headset if they experienced any discomfort and to inform the researchers of any issues. Additionally, they were regularly asked if they wished to continue or stop the test.

To accommodate these two participants, the testing procedure was modified to shorten the duration and minimize the demands placed on them. The number of focus points presented to these volunteers was therefore reduced. Given that these volunteers had recently undergone surgery and still had

postoperative wounds on their heads, it was not possible to secure the VR headset in the usual way using the head strap. Instead, the volunteers held the VR headset themselves, trying to keep it as stationary as possible in front of their eyes during the test. In order to simplify the test further, the participants were only asked to verbally confirm the detection of the approaching dots. They did not have to additionally confirm the dot entering their visual field using the Pico controller.

5. Results

This research aims to explore the feasibility of performing visual field assessments using the Peili Research app on the Pico Neo 2 Eye VR headset (VRH). A MATLAB script was developed to analyse the data collected from the app and the VRH. To achieve this objective, several sub-analyses were conducted. The test-retest reliability was investigated and the isopters obtained through the test setup were compared to those generated using the Goldmann perimeter. Additionally, two aspects of the app's design—the colour contrast of the presented target stimuli and the method used to report stimulus detection on the tablet—were examined for their potential effects on the results.

5.1 Data acquisition

Ten full datasets were obtained of a healthy volunteer with no visual field defects. During all 10 assessments, the participant was asked to click with the controller when the dots entered their visual field and provide verbal confirmation. A summary of the 10 data sets obtained from the healthy participant is provided in Table 1.

Table 1. Overview of the 10 datasets obtained from a single healthy participant.

TEST	TOTAL TIME [S]	NUMBER OF FOCUS POINTS	NUMBER OF CONTROLLER CLICKS	NUMBER OF VALIDATION POINTS	OVERALL AVERAGE GAZE DELTA [DEGREES]	OVERALL MAX GAZE DELTA [DEGREES]
1	443.90	11	36	5	1.01	9.65
2	427.00	11	36	5	0.64	1.24
3	488.90	12	40	5	0.92	1.97
4	444.65	11	36	5	1.40	25.99
5	392.61	10	34	5	0.87	2.48
6	516.15	10	33	5	1.09	4.99
7	414.28	11	36	5	0.68	1.51
8	422.27	11	36	5	0.59	1.24
9	422.59	11	36	5	0.58	1.90
10	459.59	11	37	5	0.94	22.86

The healthy participant also underwent a Goldmann visual field assessment of his left eye and his right eye. The Goldmann perimetry was performed by an experienced perimetrist at the Amsterdam University Medical Center.

Two volunteers with a known hemianopsia provided two datasets each. The test was performed differently for these volunteers. The volunteers underwent brain surgery earlier that day and the day before they performed the assessments. Due to their post-op headwounds, the VRH could not be adequately fixated on their heads with the designated head strap. Both volunteers held the VRH up to their eyes for the duration of the assessment.

5.2 Outcomes of data analyses

Analysis 1: Test-retest reliability:

The test-retest reliability of visual field measurements using the Peili Research app on the Pico Neo 2 eye was evaluated across all 10 datasets.

Figure 7 shows the exploratory plots were initially generated to allow visual inspection of the distribution and variation in theta and phi angles across tests. In addition, the average visual field limits of the 10 data sets was determined and plotted in Figure 8.

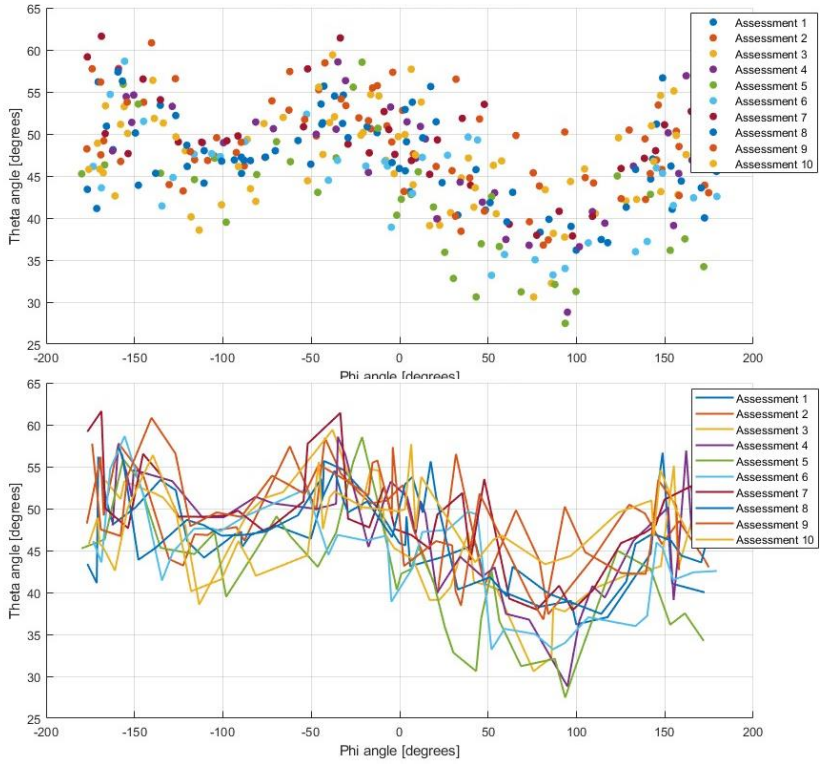

Figure 7. Exploratory plots of the 10 obtained datasets. The horizontal axis represents the phi angle, or the azimuth, in degrees. The vertical axis shows the theta angle, or elevation, which represents the visual field angle in degrees.

To accommodate the circular nature of the data, where the angle values are expected to be continuous for the entire 360 degrees, the last measurement of each dataset was appended to the start, and the first measurement was appended to the end. This approach ensured the continuity of the circular data for subsequent linear interpolation. Next, interpolation was performed to standardize the length of the data vectors, enabling a consistent basis for comparing test-retest reliability across the datasets. The interpolation also allowed the calculation of the average visual field obtained from 10 datasets.

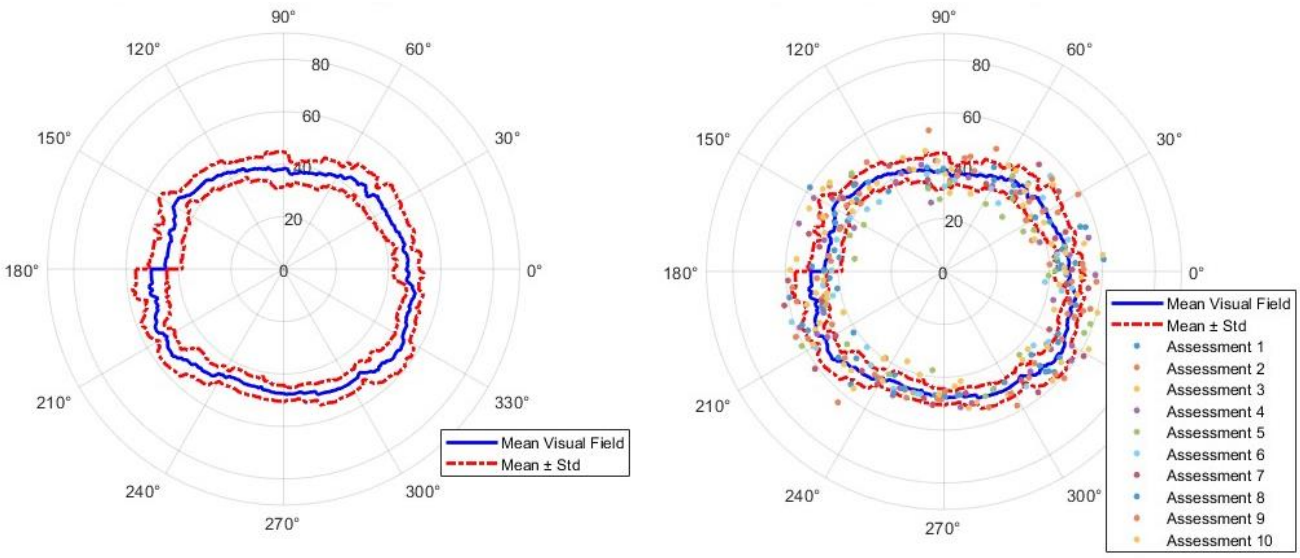

Figure 8. Isopters representing the average visual field limits calculated from 10 assessments. The blue lines represent the calculated average visual field limits. The red dotted lines represent the average +- standard deviation.

Next, the Shapiro-Wilk test was performed to assess the normality of the theta and phi angle distributions across the datasets. The results indicated that all datasets followed a normal distribution, with p-values ranging from 0.21 to 0.92. Levene's test for homogeneity of variances rejected the hypothesis (p-value: 0.013) of homogeneity in variance in the datasets. Additionally, the coefficient of variation was calculated for each dataset. Table 2 **Error! Reference source not found.** provides an overview of outcomes for each data set.

While the data followed a normal distribution, there was no homogeneity of variances. Therefore, the non-parametric Spearman correlation matrix was computed to quantify the consistency of measurements across the datasets. In Table 3 the matrix is shown. As can be seen from the table, the Spearman correlation coefficients showed variable values between -0.12 and 0.79.

The Intraclass Correlation Coefficient (ICC) was calculated to provide a measure of test-retest reliability. The ICC value obtained was 0.8398. This suggests that the Peili Research app provides consistently reliable measurements across repeated visual field tests. However, it must be noted that the statistic is less reliable because of the heterogeneity of the variances.

Table 2. Overview of outcomes for each test. The Shapiro-Wilck test indicated that each test followed a normal distribution. The mean visual field angle of all confirmed dot sightings are shown. The Coefficient of Variation is given in percentages.

TEST	DISTRIBUTION (P-VALUE)	MEAN VISUAL FIELD ANGLE [DEGREES]	STANDARD DEVIATION [DEGREES]	COEFFICIENT OF VARIATION (CV) [%]
1	Normal (0.758)	46.58	5.40	11.3
2	Normal (0.738)	48.53	5.14	9.4
3	Normal (0.495)	46.28	7.21	15.1
4	Normal (0.294)	47.37	6.87	13.4
5	Normal (0.622)	42.19	7.62	16.2
6	Normal (0.231)	44.16	6.14	13.8
7	Normal (0.210)	49.17	5.84	11.3
8	Normal (0.927)	47.66	5.02	10.0
9	Normal (0.815)	48.99	6.01	10.5
10	Normal (0.567)	47.97	4.29	7.8
TOTAL AVERAGE	**NORMAL DISTRIBUTION**	**49.89**	**5.96**	**11.9**

Table 3. Spearman correlation matrix. This shows the correlation coefficients between the datasets. The total average correlation is shown for each dataset. Positive values indicate a positive correlation; negative values indicate negative correlations, and 0 indicates no correlation.

DATASET	1	2	3	4	5	6	7	8	9	10
1	1	0,6109	0,6968	0,7904	0,7275	0,6447	0,5937	0,6795	0,7146	0,3193
2	0,6109	1	0,6297	0,5494	0,6277	0,5623	0,3906	0,5181	0,3251	0,1764
3	0,6968	0,6297	1	0,6611	0,6672	0,5568	0,7519	0,6228	0,7379	0,2546
4	0,7904	0,5494	0,6611	1	0,7267	0,6104	0,5355	0,6159	0,647	0,2581
5	0,7275	0,6277	0,6672	0,7267	1	0,5778	0,4171	0,6781	0,5953	0,2096
6	0,6447	0,5623	0,5568	0,6104	0,5778	1	0,4663	0,5827	0,4644	-0,1165
7	0,5937	0,3906	0,7519	0,5355	0,4171	0,4663	1	0,4412	0,6559	0,2796
8	0,6795	0,5181	0,6228	0,6159	0,6781	0,5827	0,4412	1	0,4526	0,1897
9	0,7146	0,3251	0,7379	0,647	0,5953	0,4644	0,6559	0,4526	1	0,2194
10	0,3193	0,1764	0,2546	0,2581	0,2096	-0,1165	0,2796	0,1897	0,2194	1
TOTAL AVERAGE	**0,57774**	**0,43902**	**0,55788**	**0,53945**	**0,5227**	**0,43489**	**0,45318**	**0,47806**	**0,48122**	**0,17902**

Analysis 2: Comparison with Goldmann perimetry

The isopters obtained using the gold standard of the Goldmann perimetry are shown in Figure 9A&B. Each eye was assessed separately, and the other eye was taped off. Two stimulus sizes were used: V and I, corresponding to 64 mm² and ¼ mm². Relative intensities were changed in steps from value 4 to 1, corresponding to 0,5,10,15 dB, respectively. During the assessment of the right eye, the perimetrist overlooked the tape that obstructed the left eye, sticking out and obscuring a small part of the visual field. This resulted in a smaller visual field in the upper left quadrant for this eye. Other than this notable observation, the Goldmann visual field assessment did not show any visual field defects.

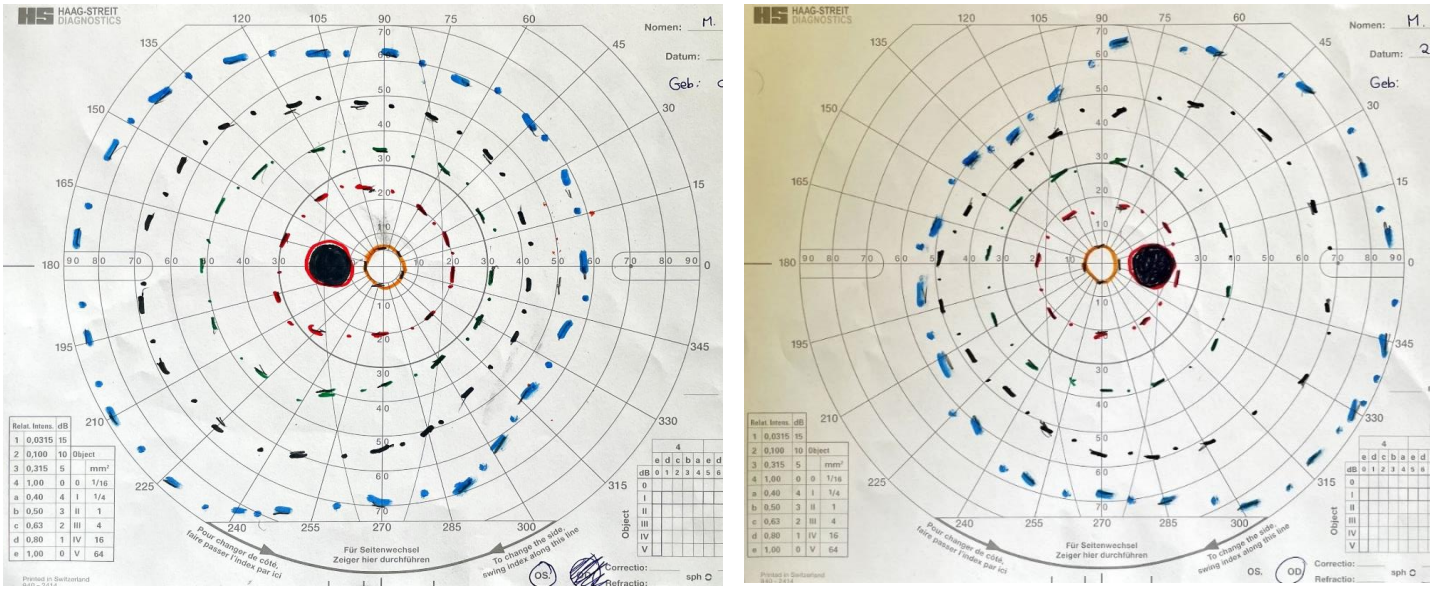

Figure 9. The Goldmann isopters of the gold standard kinetic perimetry of the healthy volunteer. Figure A (left figure) shows the isopter of the left eye. Figure B (right figure) shows the isopter of the right eye. In both isopters, the blue line represents V4, the black line represents I4, the green line represents I3, the red line represents I2, and the orange line represents I1.

The app was designed to expand the testable angle by using off-centred focal points. When participants direct their focus toward these off-centred points, and the stimulus enters from the opposite side of their visual field, the effective angle is increased. This approach should enable the app to measure the user's outer visual field limits. Determining the maximum angle that can be assessed is crucial to evaluating the feasibility of using the Peili app for visual field testing. If the angle is not increased enough, the use of off-centred focus points would be ineffective, rendering this approach futile.

Figure 10 shows a histogram of the angles of the off-centred focus point to the centre of the screen. A total of 109 focus points were tested. The analysis revealed that the average angle achieved was 23.00 degrees with a standard deviation of 11.58 degrees. The minimum angle tested was 2.45 degrees, while the maximum angle reached 50.15 degrees. The distribution of the angles achieved by the focal points is shown in the accompanying figure.

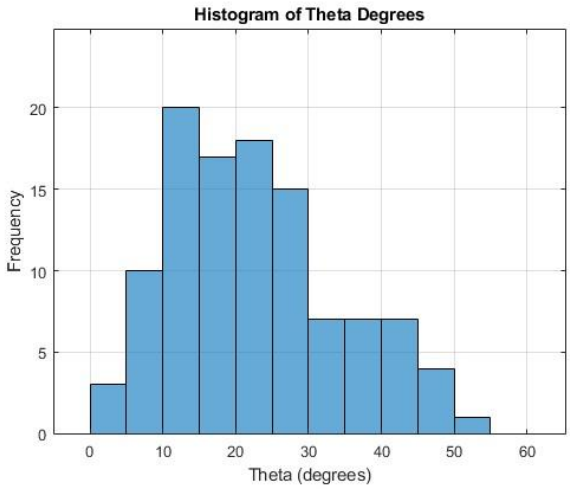

Figure 10. Histogram of the angle of the off-centred projected focus points to the centre of the screen.

Analysis 3: Human reaction time:

This analysis aims to determine whether the Peili Research app, run on the Pico Neo 2 eye VRH, can correctly map the user's visual field. The app is designed so that the detection of visual stimuli – the approaching dots – is recorded by the researcher on the tablet. However, due to the constant speed at which these dots move, it was hypothesized that the researcher's reaction time in pressing the button on the tablet might result in an underestimation of the size of the visual field.

To investigate the impact of the researcher's reaction time on resulting FOV, the time difference between confirmations made by the patient using the controller and those made by the researcher using the Peili app on the tablet was analysed. As it was not recommended to perform tests for normality in this case, histograms of the time and the angle differences were plotted to obtain a rough indication of the data distribution. (58) The histograms are visualised in Figure 11. Histograms of the differences between dot confirmations registered on the tablet by the researcher and on the controller by the participant. Figure 11. The top figure, Figure 11A, shows the distribution of the difference between the timestamps of the dot confirmation registrations. The figure on the bottom, Figure 11B, illustrates the distribution of the angle differences between confirmations made through the tablet and confirmations made using the controller.

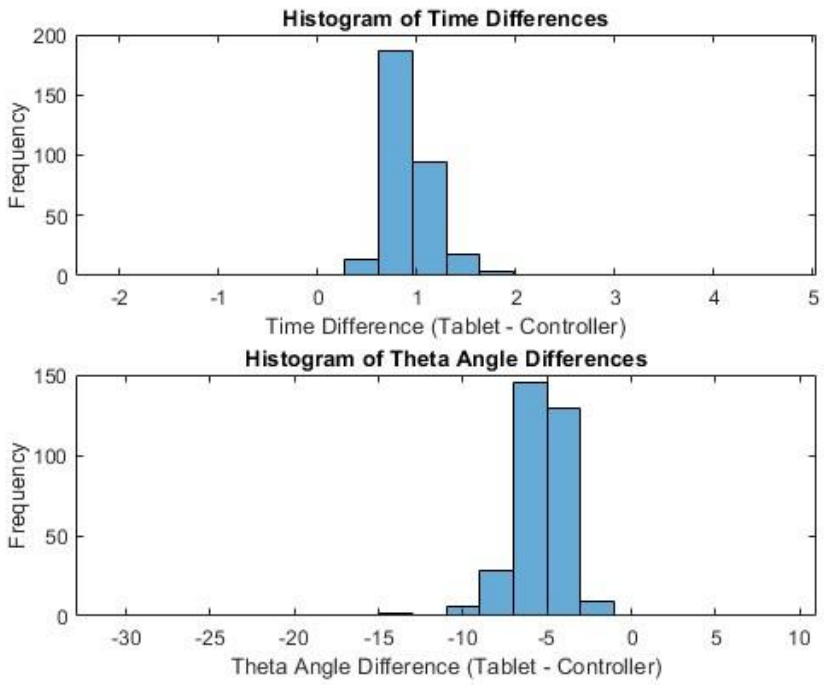

Figure 11. Histograms of the differences between dot confirmations registered on the tablet by the researcher and on the controller by the participant. Figure A (top figure) shows the time differences in seconds. Figure B (bottom figure) shows the theta visual field angle differences in degrees.

Subsequently, a paired t-test was conducted on the confirmation timestamps for each dot. The results indicated that confirmations made using the controller were significantly faster, with an average time difference of 0.94 seconds (95% CI: 0.87-0.96, $p < 0.001$). Additionally, the impact on the angular measurement of the visual field was assessed, revealing a mean theta angle difference of 5.38 degrees (95% CI: 5.11-5.76, $p < 0.001$).

An example of the difference in the isopters when confirmations are registered by the researcher on the tablet and the participant using the controller is shown in Figure 12. In this figure, the blue dots and lines show the visual field limits determined through dot detections confirmed by the participant through the controller. The red dots and lines represent the location of the dot at the timestamp the researcher registered a confirmation through the tablet. The green dotted lines represent the paths the different dots travel towards the focus point. All ten isopters obtained from the healthy participant can be found in Appendix C: Overview of isopters of all datasets from healthy volunteer.

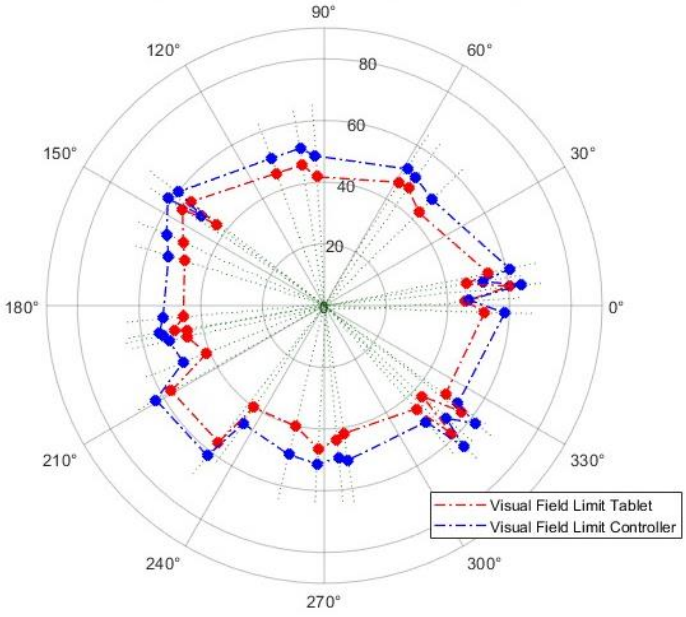

Figure 12. Visual field limits obtained by different registration methods. The blue line represents the visual field limit that was determined by the registration of dot sightings through the tablet's interface. The red line shows the visual field limits that were obtained by the particpant registrating the dot entering their visual field using the controller. The green dotted lines represent the dot trajectories.

Analysis 4: Colour contrast of the dots:

In the test performed using the Peili research app, three dots were sequentially entering the particpants visual field in three different colours. The first dot was blue, followed by the green dot, and finally, the yellow dot.

To investigate whether the colour contrast of the stimulus affects the angle at which the dots are detected, data were collected from 10 datasets, encompassing a total of 109 focus points. From these datasets, 321 dots were analysed, consisting of 107 blue, 107 green, and 107 yellow dots.

Figure 13 shows the polar plot with the positions at which the blue, green, and yellow dots were detected by participants during the test. In this figure, the stimuli are represented in their respective colours. The distribution of these dots across the visual field indicates the angular position at which each coloured target was detected. From the figure, it appears that green dots are detected at larger angles from the origin compared to the blue and yellow dots. Additionally, the green dots seem to cluster more towards the contralateral sides of the visual field, whereas the blue dots are predominantly detected in the upper right and lower left regions. The yellow dots, travelling towards the focus point were confirmed mainly in the upper left and lower right regions.

The mean visual field angles for the blue, green, and yellow dots were calculated. The mean angle for the blue dots was 42.92 degrees with a standard deviation of 5.75 degrees, the mean angle for the green dots was 53.06 degrees with a standard deviation of 5.89 degrees, and the mean angle for the yellow dots was 45.21 degrees with a standard deviation of 4.58 degrees.

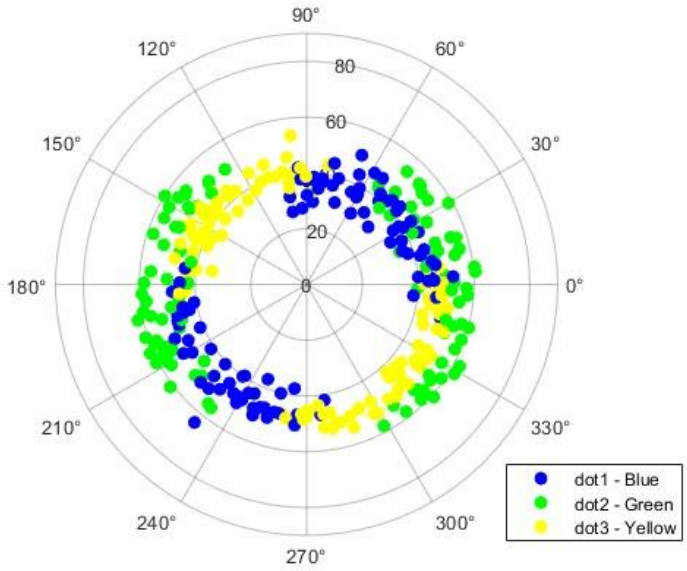

Figure 13. Polar plot of the positions of each dot's location at the time of confirmed sighting. Dot 1 is visualised in blue, dot 2 is visualised in green and dot 3 is visualised in yellow.

Following the indication of significant differences by the Friedman test, post hoc analyses were conducted between the groups using an adjusted significance level ($p < 0.01$). The post hoc analysis consisted of pairwise comparisons using the (left-tailed) Wilcoxon signed-rank test. The results of these tests revealed statistically significant differences between all pairs of colours. Specifically, the Wilcoxon test showed that the angles of the blue dots were smaller than the angles of the green dots with a z-value of -8.60 ($p<0.001$) and a signed rank of 122. Similarly, the angles of the blue were found to be smaller than those of the yellow dots with a z-value of -4.84 ($p<0.001$) and a signed rank of 1331. Finally, the yellow dots showed smaller angles than the green dots, at a z-value of -7.98 ($p<0.001$) and a signed rank of 5456.

Analysis 5: Clinical application and calibration quality

During this internship, two volunteers with known visual field defects who had recently undergone brain surgery opted to participate in this exploratory research. Collecting these volunteers' datasets also allowed identifying potential limitations to the test set-up of the Peili Research app in practice. Each volunteer was willing to perform the test twice, providing two datasets each. These datasets were used to calculate the isopters by running the data from the Peili Research app through the main script used in this research.

The isopters constructed from the datasets of the first volunteer, referred to as Volunteer A, are visualized in Figure 14. In this figure, the red dots indicate the positions of the stimuli at the moment the researcher confirmed their detection on the tablet. The blue line represents the deduced visual field limits based on the registered positions of these dots at the time of confirmation. A visual inspection reveals that the visual field angles for this volunteer range between 15 and 55 degrees in the first dataset, as shown in Figure 14A, and between 20 and 55 degrees in the second test.

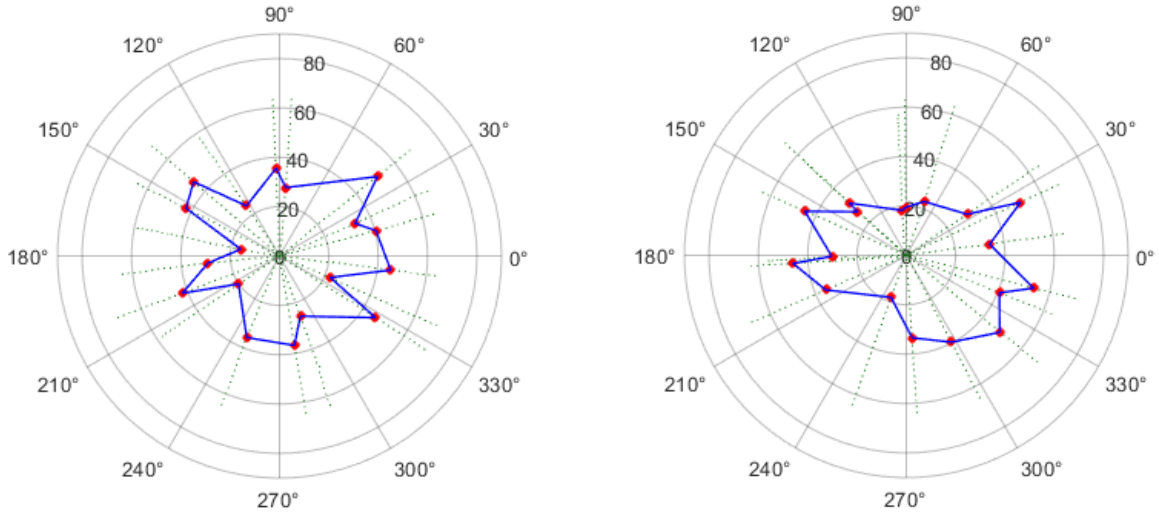

Figure 14. The isopters resulting from two tests performed by Volunteer A. The red dots represent the polar locations of the dot at the time of confirmation registration. The blue lines represent the visual field limits. The green dotted lines show the dot trajectories towards the focus point.

Similarly, Figure 15 illustrates the isopters resulting from the visual field assessment conducted on Volunteer B using the VRH. In the two tests performed, the visual field angles for this volunteer were found to range from 0 to 35 degrees.

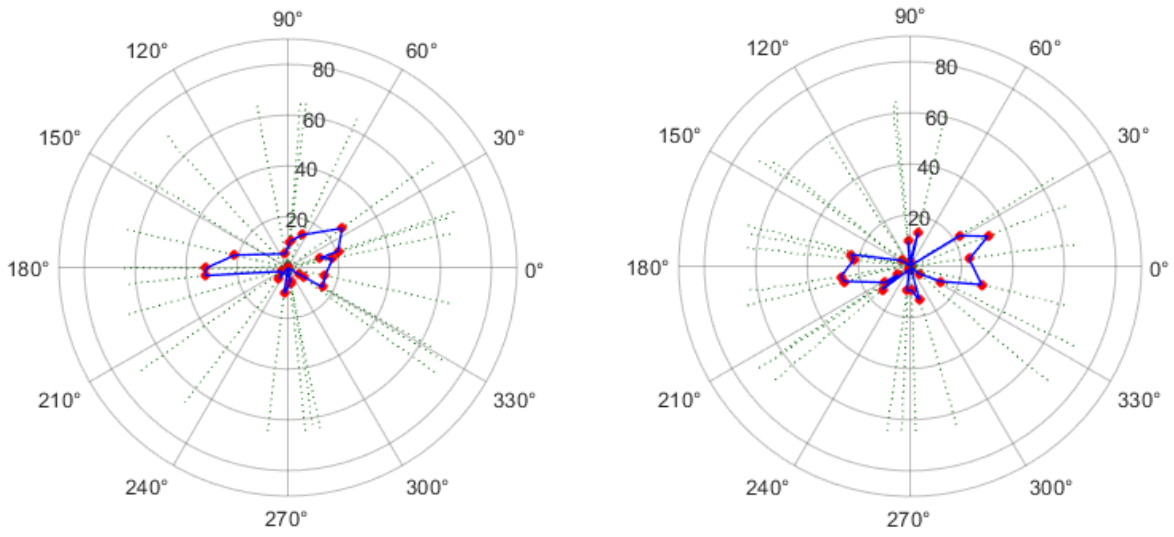

Figure 15. The isopters resulting from two tests performed by Volunteer B. The red dots represent the polar locations of the dot at the time of confirmation registration. The blue lines represent the visual field limits. The green dotted lines show the dot trajectories towards the focus point.

The tests conducted with the two postoperative volunteers raised the question of how holding the VR headset manually, instead of fixing it with a head strap, might influence the results. To explore this, a small additional test was conducted using calibration and validation methods. The healthy volunteer was asked to hold the VR headset instead of securing it with the head strap. After calibration, there was a five-minute wait before the validation process, during which the volunteer held the headset as steadily as possible in front of their eyes. The results from each validation point were carefully recorded.

Since the healthy volunteer had already provided 10 datasets where the validation was performed according to the standard protocol—immediately after calibration with the VR headset fixed in place with the head strap—this existing data was used for comparison.

Table 4 presents the results of the validation immediately following calibration with the fixed VR headset. It shows that the average errors over the 10 datasets for the individual validation points range between 0,27 and 1.39 degrees, and that the average error for each data set ranges between 0.56 and 1.39 degrees. The average error over all datasets found was 0.83 degrees.

Table 4. Results of 5-point validation performed directly after 5-point calibration by 1 healthy participant with the VRH fixed using the designated head strap.

DATASET	ERROR IN [DEGREES]					AVERAGE ERROR [DEGREES]	MAXIMUM ERROR [DEGREES]
	Validation point 1 (0°,0°)	Validation point 2 (10°,10°)	Validation point 3 (10°, -10°)	Validation point 4 (-10°,10°)	Validation point 5 (10°,-10°)		
1	0,15	0,35	1,22	0,31	2,98	1,00	9,64
2	0,24	0,76	0,99	0,35	0,82	0,63	1,24
3	0,31	0,62	1,51	0,34	1,79	0,91	1,99
4	0,42	0,19	1,26	3,77	1,32	1,39	25,99
5	0,45	0,55	1,06	0,65	1,61	0,86	2,48
6	0,58	1,12	1,70	0,39	1,62	1,08	4,99
7	0,08	0,64	1,26	0,79	0,69	0,69	1,51
8	0,27	0,65	0,88	0,11	1,02	0,59	1,23
9	0,16	0,41	0,97	0,24	1,09	0,57	1,90
10	0,06	0,42	0,82	0,56	0,93	0,56	1,32
TOTAL AVERAGE	**0,27**	**0,57**	**1,17**	**0,75**	**1,39**	**0,83**	**5,23**

Table 5 This display shows the results from the alternative method, in which the volunteer manually held the VR headset for five minutes after calibration before the validation was conducted. In this scenario, the average errors over the 10 datasets for the individual validation points range between 1.66 and 4.72 degrees. The average error found for each separate dataset ranges between 1.48 and 6.42 degrees. The average error over all datasets obtained with delayed validation was found to be 2.79 degrees.

Table 5. Results of 5-point validation performed 5 minutes after 5-point calibration by a healthy participant with the VRH manually held in place, without using the designated head strap.

DATASET	ERROR IN [DEGREES]					AVERAGE ERROR [DEGREES]	MAXIMUM ERROR [DEGREES]
	Validation point 1 (0°,0°)	Validation point 2 (10°,10°)	Validation point 3 (10°, -10°)	Validation point 4 (-10°,10°)	Validation point 5 (10°,-10°)		
1	4,71	3,52	4,70	3,26	4,89	4,22	5,48
2	1,43	1,89	0,88	0,26	3,32	1,56	11,27
3	1,54	0,78	3,46	1,35	1,61	1,75	13,14
4	0,9	0,92	2,35	0,54	2,66	1,48	17,62
5	0,51	1,06	4,77	1,42	1,13	1,78	12,33
6	0,56	2,76	0,82	1,47	10,13	3,15	19,11
7	4,14	1,05	4,77	1,79	3,68	3,09	14,6
8	5,33	2,96	1,73	0,81	2,89	2,75	19,36
9	2,95	0,78	1,06	1,93	1,89	1,72	9,55
10	5,87	4,65	2,84	3,73	14,99	6,42	33,04
TOTAL AVERAGE	**2,79**	**2,04**	**2,74**	**1,66**	**4,72**	**2,80**	**15,55**

6. Discussion

The research objective during this graduation internship was to determine if it was clinically feasible to perform a visual field assessment using the Peili Research app on a VRH. For this purpose, the foundation for an automated analysis of the examination was created in Matlab. conducted using the Peili Research application on the Pico Neo 2 eye. Several analyses were performed to provide a comprehensive answer to the research question. The test-retest reliability was investigated, the results were compared with the gold standard for Kinetic Perimetry and two aspects of the application's design were investigated: the effect of human reaction time and the effect of the stimulus colours. In addition, the clinical application and its impact on eye-tracking calibration quality were explored.

6.1 Primary outcomes

Analysis 1: Test-retest Reliability

The test-retest reliability of visual field measurements using the Peili Research app on the Pico Neo 2 Eye was evaluated across 10 datasets to determine the app's consistency in producing reliable results. The exploratory plots, visualised in Figure 7, provided a visual overview of the distribution and variation in theta across the tests. These plots indicated some degree of variability, prompting further statistical analysis to quantify the reliability of the measurements.

The Shapiro-Wilk test was performed to assess the normality of the theta and phi angle distributions. It revealed that all datasets followed a normal distribution, with p-values well above the threshold of significance. However, Levene's test for homogeneity of variance indicated that the data did not meet the criteria for using parametric methods. Therefore, the non-parametric Spearman correlation matrix was calculated to determine the consistency of measurements.

The matrix showed correlation coefficients ranging from -0.12 to 0.79, indicating poor to moderate correlations between the datasets. Most coefficients were below 0.6, and several were close to zero, indicating weak relationships. These findings imply that the measurements across datasets may not be reliably consistent, highlighting potential variability or inconsistency in the test results.

To provide a comprehensive measure of test-retest reliability, the Intraclass Correlation Coefficient (ICC) was calculated, yielding a value of 0.8398. This high ICC value suggests that the Peili Research app generally provides consistent and reliable measurements across repeated visual field tests. However, the

ICC generally assumes normality and low variety. The heterogeneity of the variation observed, and Spearman correlations indicate that this statistic is most likely not reliable. While the app performs reliably in most cases, there may be instances where variability in measurements could impact the overall reliability.

However, when inspecting Figure 8, the data does seem to follow a pattern. It is possible that there was not enough data collected to correctly determine the correlation through statistics.

Analysis 2: Comparison with Goldmann perimetry

When comparing the isopters resulting from the Peili Research app with the isopters obtained through Goldmann perimetry, the VR-obtained results show smaller visual field limits. However, no statistical tests were conducted to compare these results correctly.

It is understandable that the visual field limits observed with the Peili app do not precisely match those found using the Goldmann perimetry method. As discussed in the technical background, the FOV advertised by VR headsets is often measured under ideal conditions and does not account for individual anatomical variations, such as eye relief distance. However, this was expected to influence results, so the app was designed to increase the visual angle tested. Its efficacy in doing so is, therefore, a key factor in the objective of observing the limits of the participant's visual field.

The effectiveness of the Peili app in expanding the visual field angles tested by using off-centred focal points was investigated. When participants focus on these off-centred points, and the stimulus enters from the opposite side of the visual field, the effective angle being tested increases. This method is intended to enable the app to measure the outer limits of the user's visual field.

The analysis tested 109 focus points and found that the average angle to the centre of the projection was 23.00 degrees.

Sauer et al. reported that the Pico Neo 2 headset reached a mean FOV of between 86 and 88 degrees, corresponding to about 44 degrees per hemifield. (44) During this research, the app was able to measure a maximum visual angle of approximately 68 degrees per hemifield in a healthy participant. Although this is larger than the FOV reported by Sauer et al., it falls short of the targeted 90 degrees for the human visual field limit. This limitation is likely due to the focal points not always being projected at the extreme edges of the visual field, which prevented the app from testing the maximum possible angles. This aspect of the app’s design needs improvement to fully capitalize on the potential of off-centred focal points.

Overall, the results indicate that the Peili app can indeed expand the testable visual field angle beyond the typical FOV reported by Sauer. However, while the design of the Peili app is able to increase the effective visual field angle tested beyond the typical FOV reported by Sauer, it does not do so sufficiently. To properly test the outer peripheral limits of the participant's visual field, the focus points should be projected at a larger angle from the centre.

Moreover, as was shown in Figure 10, the angle at which the focus point is shown can vary. When not all focus points are shown at the same distance or angle from the centre of the screen, the tested angles and, thereby, the visual field examination performed are not the same for each assessment. This affects the

test-retest reliability analysis as the same test is not executed twice. This may account for the variance and low correlation coefficients that were found during the test-retest reliability analysis.

Analysis 3: Human reaction time

To determine if it is clinically feasible to use the Peili Research app on the Pico Neo 2 eye for mapping the user's visual field, it is essential to identify any aspects of the current test set-up and app design that may lead to a bias. This analysis aimed to identify and quantify the effect of the chosen approach to record the limits of the visual field.

In the Peili app on the VRH, the stimulus moves at a constant, hardcoded speed. This makes the time it takes the participant to verbalize dot sightings and the time it takes the researcher to record the confirmation more significant. The current design of the app running on the VRH and the tablet requires the researcher to record the detection of visual stimuli (moving dots) on a tablet, as opposed to the participants recording dot detection themselves.

This process was explored by comparing two methods of recording confirmed sighting of the stimulus: one where the participant presses a button on the controller upon detecting the stimulus, and another where the researcher records verbal feedback from the participant in the tablet app.

The analysis revealed that the extra step in the current design of the Peili app—where the participant verbally confirms detection and the researcher records this input—introduces an unnecessary delay. Specifically, the participant's direct input via the controller was nearly one second faster than the researcher-recorded input, resulting in a potential underestimation of the visual field by more than 5 degrees. This suggests that using the tablet method for confirming stimulus detection could result in an isopter showing a total visual field that is over 10 degrees smaller than it is.

These findings are significant for clinical practice, as they suggest that the current setup does not provide an accurate representation of a patient's visual field, potentially leading to incorrect diagnoses or assessments.

Analysis 4: Colour contrast of the dots

It was hypothesized that the colour (contrast) of the dots may have an influence on the angle at which they were detected. This analysis confirmed that there are differences between the angles of the blue, green, and yellow dots as they were detected by participants across the visual field. The findings revealed that green dots were detected at larger angles compared to blue and yellow dots.

The earlier detection of the green dots may be attributed to the human spectral sensitivity. The human eye is most sensitive to green light, which coincides with the peak sensitivity of the vision system under well-lit conditions. (59, 60) This heightened sensitivity to green allows the visual system to detect green targets more effectively, even at more peripheral angles. This seems consistent with the polar plot results, where green dots were more often detected earlier at larger angles. In contrast, human sensitivity to blue light lies near the lower range of the human visual spectrum. The lower sensitivity to blue light, combined with the moderate contrast provided by the blue and grey background used in the experiment, likely decreased the detectability of blue dots.

The yellow dots, although detected at larger angles than the blue dots, were not detected as widely as the green dots. This can be attributed to the human eye's sensitivity hierarchy, where yellow light is detected more easily than blue but not as efficiently as green. The contrast between the yellow dots and the background was sufficient to allow for broader detection than the blue dots but did not extend as far as the green dots.

The significant differences between the detection angles of the blue, green, and yellow dots, as confirmed by the Wilcoxon signed-rank test, are in line with the hypothesis that the colour contrast of the presented stimuli influences the results of the visual field assessment conducted with the Peili Research app. However, two other important aspects of the app's design must be taken into account.

First, as was seen in Figure 13, the distribution of the dot locations at their detection appears to be aligned in a 180-degree pattern across the visual field. This distribution can be attributed to the test design, particularly the semi-automatic placement of the off-centred focus points. These focus points were systematically positioned in the upper, middle, and lower regions, either to the left or right. Based on the visual pattern observed and on Figure 5, which was provided with the supplementary material of the Peili Research app, it seems likely that the path of the green dots always crosses the centre of the visual field as they move towards the off-centred focus points. This consistent crossing of the centre by the green dots could explain why they are more often detected on the sides of the visual field. In contrast, the blue and yellow dots follow trajectories at a 45-degree angle to the green trajectory. Their trajectory will then not cross the central axis in the testing environment and are, therefore, more pronounced in specific visual field areas.

In addition, the fixed order in which the dots were presented may have also influenced the results of this analysis. While it is possible that the differences in the angles between the three dots may be attributed to the colour contrast of the dots, the sequential presentation may have also affected the participant's response. Factors such as anticipation, learning effects, or fatigue have not been investigated in this research. During the test, the healthy participant mentioned becoming accustomed to the task and had a rough idea of where the next dot would appear. This may have improved reaction times for subsequent dots. In general, this could lead to an underestimation of the detection angle for the first (blue) dot, as participants might not be fully attuned to the task at the beginning of the sequence. Conversely, the green and yellow dots, which are presented later, might benefit from the participants' increased focus and familiarity with the task.

Analysis 5: Clinical application and calibration quality

The results obtained from the two postoperative volunteers provided valuable insights into the practical challenges associated with using the Peili Research app on the Pico Neo 2 Eye for visual field assessments in a clinical setting. The isopters generated for Volunteer A showed visual field angles ranging from 15 to 55 degrees, while those for Volunteer B were smaller, ranging from 0 to 35 degrees. Upon visual inspection of their respective isopters, it seemed that volunteer B had a more pronounced visual field defect. Additionally, the isopters from both patients seem to be smaller when visually comparing them to the isopters of the healthy participant. This may suggest that the Peili Research app is able to detect a compromised visual field. However, this cannot be stated for certain as no statistical analysis was performed.

A key concern identified while conducting the test with the post-operative volunteers was the necessity for the participants to manually hold the VR headset to their eyes. This was required due to their postoperative head wounds, which prevented them from fixating the VRH with the head strap. This prompted the question of whether this may have an influence on the accuracy of the results.

To explore this further, the healthy volunteer was asked to conduct 10 more calibrations and validations with the VRH. This time, the validation would be completed after manually holding the VRH in place without the head strap for 5 minutes. The validation results from the healthy volunteer's complete assessment, where validation was performed immediately after calibration and with the VRH fixated using the head strap. When the VR headset was held manually for 5 minutes, the average error in validation increased significantly, from 0.83 degrees (with the headset fixed) to 2.80 degrees (with the headset held manually). This increase in error suggests that the stability of the headset is crucial for obtaining accurate eye-tracking data. The errors observed during the manual holding condition were not only higher but also more variable, indicating that even slight movements of the headset can lead to substantial inaccuracies in the visual field measurements.

These findings have important implications for the clinical applicability of the Peili Research app. In scenarios where the headset cannot be securely fixed, the reliability of the visual field data may be compromised. This limitation could negate the potential benefits of using VR-based assessments in clinical contexts where proper fixation of the VRH is not possible.

6.2 Study limitations and recommended improvements

A number of general limitations can be found in the research performed during this graduation internship. First, this study only included a single participant and generated just 10 data sets, each containing approximately 11 focus points with around three dot confirmations per set. This limited sample size significantly restricts the generalizability of the results and limits the statistical power of the analysis. Additionally, the current investigation did not perform a statistical comparison with the Goldmann perimetry.

Besides these general limitations, this feasibility study also faced a number of other challenges. The limitations related to the application software, the hardware, and the clinical applicability will be discussed.

Test set up

Performing visual field assessments with the Peili Research app on the Pico Neo 2 Eye VRH in the current set-up is accompanied by several limitations that could impact the reliability or accuracy of the gathered data.

The Peili Research app was designed to perform kinetic visual field assessments on a VRH, even though this VRH has a smaller FOV than the human FOV. It aims to do so by increasing the effective angle tested through the use of off-centred focus points. However, in its current design, the position of where the focus points must be located is set semi-automatically. The researcher can request an area of interest, e.g. “upper left” or “lower right”, but cannot manually set the distance to the centre of the screen. As shown in analysis 2 in this research, this often means that the effective visual field angle tested is not increased

sufficiently. It was found that focus points were shown at an angle of around 23 degrees from the centre, thereby only increasing the effective angle with 23 degrees. As was found by Sauer et al., the Pico Neo 2 eye only has an average effective FOV of 88 degrees (44 degrees peripheral). (44) Combining these two values means that the average effective angle that can be tested using the Peili Research app on the Pico Neo 2 eye is around 67 degrees, while 90 degrees would be appropriate. It is recommended that the focus points are projected in the outer fields of the screen to be able to correctly assess the outer limits of the participant's visual field.

The Peili Research app does not allow the researcher to vary in dot characteristics such as size, colour, or speed. Specifically, the difference in colour contrast between the dots used during the assessment also introduces variability, as the human eye is more sensitive to green light. This could lead to biased results, where green stimuli are detected more readily than others, skewing the visual field assessment. It would be advantageous for the app to include options for adjusting the colours, luminance, size and speed of the approaching dots. This feature would offer greater flexibility and precision in the visual stimuli used during testing.

Similarly, the background in the virtual testing environment is not an even colour but a blue sky with clouds fading to grey. This could affect the detection of the blue dots, particularly due to the lower colour contrast. In addition to contrast, brightness and luminance are also crucial factors in human vision and the ability to detect stimuli, as evidenced by Goldmann perimetry, where variations in luminance levels are varied to investigate sensitivity boundaries. Currently, the headset's brightness is adjustable, but no recommended settings are provided, and the effects of using different brightness levels on the assessment outcomes remain unknown. Addressing these issues by providing guidance on optimal brightness settings and enhancing the app's capabilities could lead to more accurate and reliable visual field assessments.

As previously reported, the Pico Neo 2 Eye uses foveated rendering, a technique that reduces the resolution in the peripheral areas to optimize performance. Upon initializing the headset, static foveated rendering is indeed observed when gazing towards the corners of the screen. However, this feature is not mentioned or clarified in the supplementary document, leaving an important gap in understanding the app's capabilities and limitations. With the objective of the test performed through the Peili app, the peripheral visual fields are specific regions of interest; a lower peripheral resolution is not desired. It is currently unknown whether the Peili app can turn off the standard foveated rendering feature on the Pico device. If the app does not override or disable foveated rendering, the approaching dots to be observed may displayed at a lower resolution and appear blurry and with less contrast or sharpness with respect to the background. This may result in delayed detection of approaching dots, thereby affecting the precision of the visual field assessment. It is recommended that confirmation is obtained whether the foveated rendering is or can be overruled in the Peili Research environment.

In the execution of a Goldmann visual field assessment, the perimetrist controls the speed of the stimulus, slowing it down as the expected visual field limit is approached, thereby minimizing effects due to human reaction time. In contrast, on the VRH, the stimulus moves at a constant, hardcoded speed. This makes the reaction time of both the researcher, who must press a button on a tablet, and the participant, who must confirm the detection of the stimulus, much more significant. As observed in analysis 3, the current design of the combined app running on the VRH and the tablet introduces a significant delay of

approximately 1 second due to the reaction time of the researcher. When the participant was asked to confirm the dot entering their visual field using the controller – as opposed to verbalizing this for the researcher to register in the app – the visual field angle that was found was around 5 degrees larger. It should, therefore, be considered that the confirmation method in the test setup is changed, and the participant should report dot sightings using the available controller.

Furthermore, unlike standard visual field tests where each eye is tested separately, the Peili Research app assesses both eyes simultaneously through the VRH. This deviates from the conventional Goldmann perimetry, complicating the fair comparison of the isopters. Previous research performing static perimetry demonstrated that each eye can be assessed separately by projecting the stimulus on one of the two displays in the VRH. (16) This approach can be considered for the Peili Research app to allow for testing each eye separately.

All positional and directional data that can be subtracted from the VRH after an assessment are stored in world coordinates. The technical background section described the two methods for fusing eye-tracking and head position into world coordinates. The first method was using current head position data and current eye tracking data, which is more accurate but may lead to lagging real-time visualisation of the gaze. The other approach is by forward projecting historical head position data into the eye tracking data. This is generally less accurate, particularly during sudden head movements, but does allow for real-time gaze visualisation without any delay. During Matlab analysis, a few dots were found to have unstable trajectories and were removed for further analysis. This may indicate that the Pico Neo 2 eye and the Peili Research app have used forward projection to fuse eye-tracking and head pose data. As previously discussed, this may lead to inaccuracies in the eye-tracking world coordinates. It is worth considering opting for the alternative approach for fusing head pose and gaze data. While the alternative may lead to a slight lag in real-time visualisations of the user's gaze, it is more accurate for analysis afterwards.

Furthermore, the Matlab script developed during this research relies on dot trajectories to determine the location of the focus point. When these dot trajectories are unstable, it becomes difficult to accurately determine the focus point's location, leading to incorrect rotation of the coordinate system. These rotations are critical for subsequent calculations, such as determining the angles of the visual field. If the rotations are not accurately computed due to unstable trajectories, the results of the visual field assessment may be compromised and ultimately unusable. Prioritizing accuracy in data analysis is crucial for ensuring the reliability of the results obtained from the VR-based assessments.

Currently, analysis is conducted post-test, but the clinical value of VR-based testing would be significantly enhanced if results could be generated and reviewed in real-time. This feature would also be vital for future bedside or intraoperative applications, as discussed in the introduction. The Peili Research app could become a more powerful tool for visual field testing if results were available immediately. If this improvement is made, however, the current approach for fusing eye-tracking and head pose into world coordinates may be sufficient.

Practical limitations during tests

The Peili Research app and the Pico Neo 2 eye presented a few practical limitations to the smooth conduction of the full assessment.

Before starting the test, the first issue can arise during the calibration and validation procedure of the eye-tracker. After the calibration step of the Peili Research app, the researcher is not alerted that the calibration is finished and that the validation process can be started. This is only visualised on the VRH interface, consequently, researchers are compelled to repeatedly inquire the participants about their perceived stimuli during these phases. In addition, sometimes, the participant is instructed in the VR environment to adjust the headset. The researcher is not informed of this, and does not know the specific adjustment that is required. This interferes with the smooth execution of the calibration and validation process.

Another limitation can be found in the incomplete real-time visualization for researchers due to insufficient correction for the difference in screen size between the tablet and the VRH. Correction for this difference is not done correctly and a discrepancy can occur. This was discovered during a preliminary test, during which an advancing dot was already observable to the participant within the VRH environment but was not yet detectable on the tablet's screen used by the researcher. This discrepancy necessitates frequent communication between the researcher and participant to confirm what is being shown on the VRH, which can disrupt the flow of the assessment. Aligning these visualizations will help researchers better understand the participant's experience and will allow for a smooth conduction of the assessments.

While performing the assessment on two post-operative patient's bedsides, an essential limitation to the clinical applicability of the current test set-up was identified. Due to the head wounds from surgery, it was not possible to fixate the VRH correctly using the head strap. To overcome this, these two volunteers were asked to manually hold the VR headset in place. Over time, the patients became tired and reported difficulty in keeping the headset stable, resulting in minor and frequent readjustments. These movements affected the accuracy of the collected eye-tracking data. The accuracy of the data obtained through the calibration procedures is known to deteriorate over time but decreased more rapidly by these movements. Analysis 5 showed that the average error of the eye tracking data decreased by approximately 2 degrees when validation was performed after holding the VRH in place for 5 minutes. From this, it can be expected that the results obtained under these circumstances will also be less accurate, which may negate any potential advantages gained from performing the visual field assessments in combination with eye-tracking technology.

Moreover, the Pico Neo 2 eye was prone to overheating. Overall, it was possible to perform one full assessment with the VRH, but conducting two complete tests as described in Appendix B: Manual for Peili app consecutively was often interrupted by a notification on the VRH that the headset was overheated. The headset shut down shortly after this message.

Data analysis

The limitations associated with the obtained data have posed significant challenges to the interpretation and analysis process due to the initial absence of accompanying documentation or a readme file. As a result, a substantial amount of research time was devoted to deciphering the data and locating specific information within the files. Uncertainties regarding the variables and their representations posed some initial difficulties. For instance, the presence of different timestamps, such as "TimeSinceStartup,"

"TimeStamp,", “time”, and "PeiliEventTime", proved to be comprehended during analysis and resulted in cumbersome approaches during the interpretation and analysis of the data. A number of variables seemed to indicate the position of the focus point: “focus point relative to the camera”, “last gaze hit point”, or “gaze hit point”. The absence of clear definitions clouded the data's intuitive interpretation and introduced an unnecessary risk of inaccuracies in the performed analysis.

However, after several requests, the developers eventually provided supplementary material, which is provided in Appendix A: AUMC Neuro app supplementary document, that confirmed most of the definitions used in this research. Despite the supplementary material, some uncertainties regarding the location of the focus points persisted, particularly concerning the accurate interpretation of the "focus point relative to camera" variable. In the current script, the focus point is determined by the endpoint of the dot trajectories. However, this approach presents several limitations that need to be addressed. Data extracted from the VRH contained the focus point relative to the camera value. However, exploratory plots revealed discrepancies between the expected and observed focus points. These plots showed that the dots did not approach the coordinates of this focus point. While several attempts were made, it remains unclear how to effectively translate this focus point relative to the camera into the correct coordinate system. It was, therefore, decided to use the endpoint of the dot trajectories as the focus point. Unfortunately, this approach requires the dot to complete its entire trajectory to accurately determine the focus point, even if the dot is detected much earlier. Given that a single dot's trajectory lasts 10 seconds, assessing one focus point can take more than 30 seconds. This unnecessarily prolongs the testing process, thereby reducing its clinical value.

Given these considerations, the current method of determining the focus point by using the endpoint of dot trajectories may not be the most efficient or clinically relevant approach. Further refinement of the method is necessary to enhance both the accuracy and practical application of the visual field assessments.

In this research, blinks were excluded from the analysis because they do not contain relevant information for the visual field assessment. The eye-tracking technology used in the study automatically identifies when an eye is closed and labels these data points as invalid. However, since the eye also makes movements immediately before and after a blink, additional data points surrounding the invalid ones were also removed to account for this. The average duration of the blink was used as an indication for the margins of the samples to be removed. (55) Despite these precautions, as shown in Figure 6, the blink movement is not always entirely eliminated from the data. A conservative approach was deliberately chosen in order to avoid discarding too much potentially valuable data. This method aims to strike a balance between removing noise caused by blinks and retaining as much useful information as possible for accurate analysis. It can be considered to increase the set duration of the blink.

6.3 Future research

To build upon the findings of this research, future studies should focus on improving the Peili Research app, especially after implementing the recommendations discussed earlier. Conducting a larger-scale study is crucial to assess the test-retest reliability, determine the accuracy, and evaluate the clinical applicability of the improved app, particularly in the operating room setting.

Moreover, future research should explore the use of varying luminance levels and other parameters to investigate the potential of kinetic perimetry within the limited FOV of the VR headset. Given the constraints of the headset's FOV, perimetry could offer more precise testing options. Additionally, maintaining a uniform background, rather than the current sky with clouds, could improve colour contrast and, consequently, the accuracy of visual field assessments.

It is recommended to evaluate the clinical applicability and value of the app. Since the validation of the eye-tracking data deteriorates quickly, the current form of the test may not provide better outcomes than simpler, quicker methods like the Donders test. Therefore, a careful balance between time efficiency and the quality of results must be considered.

Expanding beyond perimetry, future investigations should explore other ocular assessments and neuropsychological tests that could be conducted using VR and eye-tracking technologies. This could include developing new tests for language, attention, and other cognitive functions, potentially revolutionizing neuropsychological testing by integrating VRH and eye-tracking. The potential for creating entirely new neuropsychological assessments using these technologies is significant, offering a new frontier for research and clinical practice.

7. Conclusion

This research aimed to evaluate the clinical feasibility of using the Peili Research app on the Pico Neo 2 eye for visual field assessment, particularly in determining visual field limits and identifying potential visual field defects. The findings indicate that in its current form, the Peili Research app is not yet suitable for accurate visual field testing. The primary limitation is that the focus points are not projected far enough towards the periphery, thereby not increasing the effective angle tested.

The research addressed several key questions to assess the app's performance. First, the test-retest reliability of the test results was evaluated by having the same participant perform the test multiple times. Spearman correlation coefficients varied considerably, and the average coefficient of variance was close to 12%. Second, the results from the visual field assessment performed through the Peili Research app did not fully align with the results from the Goldmann Perimetry. This can be attributed to the app's insufficient increasing the effective testable angle. Third, the study examined the influence of human reaction times on test results. It was found that there is a significant difference—approximately one second—between confirming the visual stimulus verbally and physically, which can lead to a discrepancy of about 5 degrees in the visual field limit found for a single hemifield. Fourth, the effect of dot colour contrast was analysed. The study confirmed that the colour of the moving dots—blue, green, and yellow—affects the angles at which they are detected. This suggests that both colour contrast and the sequence of dot presentation play roles in the visual field test outcomes. Finally, the research explored the clinical application and calibration quality of the VRH. The VR-obtained isopters from two volunteers with a known visual field defect showed smaller visual field limits, indicating that the Peili Research app can detect severe visual field defects. It was observed that in clinical practice, particularly with neurosurgical patients who may have head wounds, the need to hold the VR headset manually significantly degrades the quality of eye-tracking data, making the data less reliable for analysis. This finding underscores the challenges of using VR-based visual field testing in clinical settings, especially in cases where the headset cannot be securely fixed.

In conclusion, while the Peili Research app provides a novel approach to visual field assessment, several technical and methodological limitations must be addressed to ensure accurate and reliable data collection. In its current form, the app is not yet clinically feasible. However, with a number of changes and clarifications to the software, it is expected that the results will improve a lot. With further research after the application improvements, it may be feasible to use the application in clinical practice.

References

1. Delion M, Terminassian A, Lehousse T, Aubin G, Malka J, N'Guyen S, et al. Specificities of Awake Craniotomy and Brain Mapping in Children for Resection of Supratentorial Tumors in the Language Area. World neurosurgery. 2015;84(6):1645-52.
2. Duffau H. Resecting diffuse low-grade gliomas to the boundaries of brain functions: a new concept in surgical neuro-oncology. Journal of neurosurgical sciences. 2015;59(4):361-71.
3. Freyschlag CF, Duffau H. Awake brain mapping of cortex and subcortical pathways in brain tumor surgery. Journal of neurosurgical sciences. 2014;58(4):199-213.
4. Fernández Coello A, Moritz-Gasser S, Martino J, Martinoni M, Matsuda R, Duffau H. Selection of intraoperative tasks for awake mapping based on relationships between tumor location and functional networks. Journal of neurosurgery. 2013;119(6):1380-94.
5. Ruis CJJoc, neuropsychology e. Monitoring cognition during awake brain surgery in adults: a systematic review. 2018;40(10):1081-104.
6. Zaed I, Chibbaro S, Ganau M, Tinterri B, Bossi B, Peschillo S, et al. Simulation and virtual reality in intracranial aneurysms neurosurgical training: a systematic review. Journal of neurosurgical sciences. 2022;66(6):494-500.
7. Alashram AR, Padua E, Annino G. Virtual reality for balance and mobility rehabilitation following traumatic brain injury: A systematic review of randomized controlled trials. Journal of clinical neuroscience : official journal of the Neurosurgical Society of Australasia. 2022;105:115-21.
8. Mazerand E, Le Renard M, Hue S, Lemée JM, Klinger E, Menei P. Intraoperative Subcortical Electrical Mapping of the Optic Tract in Awake Surgery Using a Virtual Reality Headset. World neurosurgery. 2017;97:424-30.
9. Bernard F, Clavreul A, Casanova M, Besnard J, Lemée JM, Soulard G, et al. Virtual Reality-Assisted Awake Craniotomy: A Retrospective Study. Cancers. 2023;15(3).
10. Hansen DW, Ji Q. In the eye of the beholder: a survey of models for eyes and gaze. IEEE transactions on pattern analysis and machine intelligence. 2010;32(3):478-500.
11. Clay V, König P, König S. Eye Tracking in Virtual Reality. Journal of eye movement research. 2019;12(1).
12. Howard IP, Rogers BJ. Binocular vision and stereopsis: Oxford University Press, USA; 1995.
13. Schiefer U, Pätzold J, Dannheim F, Artes P, Hart WJO. Conventional perimetry. 2005;102(6):627-46.
14. Swienton DJ, Thomas AG. The Visual Pathway—Functional Anatomy and Pathology. Seminars in Ultrasound, CT and MRI. 2014;35(5):487-503.
15. Dersu I, Wiggins MN, Luther A, Harper R, Chacko JJJoOMT. Understanding visual fields, part I; Goldmann perimetry. 2006;2(2).
16. Terracciano R, Mascolo A, Venturo L, Guidi F, Vaira M, Eandi CM, et al. Kinetic perimetry on virtual reality headset. 2023;17(3):413-9.
17. Pennebaker G, Stewart W, Stewart J, Hunt HJE. The effect of stimulus duration upon the components of fluctuation in static automated perimetry. 1992;6(4):353-5.
18. Goldmann HJO. Grundlagen exakter perimetrie. 1945;109(2-3):57-70.
19. Goldmann HJO. Ein selbstregistrierendes Projektionskugelperimeter. 1945;109(2-3):71-9.
20. Goldmann HJO. Demonstration unseres neuen Projektionskugelperimeters samt theoretischen und klinischen Bemerkungen über Perimetrie. 1946;111(2-3):187-92.
21. Johnson CA, Keltner JL. Optimal rates of movement for kinetic perimetry. Archives of ophthalmology (Chicago, Ill : 1960). 1987;105(1):73-5.

22. Hirasawa K, Shoji N, Okada A, Takano K, Tomioka S. Evaluation of stimulus velocity in automated kinetic perimetry in young healthy participants. Vision research. 2014;98:83-8.
23. Wabbels B, Kolling GJDOZdDOG. Automated kinetic perimetry using different stimulus velocities. 2001;98(2):168-73.
24. Hart W, Hartz R, Hagen R, Clark KJIo, science v. Color contrast perimetry. 1984;25(4):400-13.
25. Hart Jr WM, Gordon MOJO. Color perimetry of glaucomatous visual field defects. 1984;91(4):338-46.
26. Chang DF. Chapter 2. Ophthalmologic Examination. In: Riordan-Eva P, Cunningham ET, editors. Vaughan & Asbury's General Ophthalmology, 18e. New York, NY: The McGraw-Hill Companies; 2011.
27. Niederhauser S, Mojon DS. Normal Isopter Position in the Peripheral Visual Field in Goldmann Kinetic Perimetry. Ophthalmologica. 2003;216(6):406-8.
28. Portengen BL, Porro GL, Bergsma D, Veldman EJ, Imhof SM, Naber MJE, et al. Effects of stimulus luminance, stimulus color and intra-stimulus color contrast on visual field mapping in neurologically impaired adults using flicker pupil perimetry. 2023:77-89.
29. Nowomiejska K, Vonthein R, Paetzold J, Zagorski Z, Kardon R, Schiefer UJO. Comparison between semiautomated kinetic perimetry and conventional Goldmann manual kinetic perimetry in advanced visual field loss. 2005;112(8):1343-54.
30. Wilscher S, Wabbels B, Lorenz BJGsAfC, Ophthalmology E. Feasibility and outcome of automated kinetic perimetry in children. 2010;248:1493-500.
31. Spector RH. Visual Fields. In: Walker HK, Hall WD, Hurst JW, editors. Clinical Methods: The History, Physical, and Laboratory Examinations. Boston: Butterworths

Copyright © 1990, Butterworth Publishers, a division of Reed Publishing.; 1990.
32. Gonzalez F, Perez R. Neural mechanisms underlying stereoscopic vision. Progress in Neurobiology. 1998;55(3):191-224.
33. Razek MHAJASEJ. Refraction of light and its applications. 2020.
34. Tobii. Coordinate Systems: Tobii XR Devzone; [Available from: https://developer.tobii.com/xr/learn/technical-information/coordinate-systems/#fusing-eye-tracking-and-head-pose.
35. Meehan M, Razzaque S, Whitton MC, Brooks FP, editors. Effect of latency on presence in stressful virtual environments. IEEE Virtual Reality, 2003 Proceedings; 2003: IEEE.
36. Duh HB-L, Lin JJW, Kenyon RV, Parker DE, Furness TA. Effects of Characteristics of Image Quality in an Immersive Environment. Presence: Teleoperators and Virtual Environments. 2002;11(3):324-32.
37. Brunnström K, Dima E, Qureshi T, Johanson M, Andersson M, Sjöström M. Latency impact on Quality of Experience in a virtual reality simulator for remote control of machines. Signal Processing: Image Communication. 2020;89:116005.
38. Stauffert J-P, Niebling F, Latoschik MEJFiVR. Latency and cybersickness: Impact, causes, and measures. A review. 2020;1:582204.
39. Chang E, Kim HT, Yoo BJIJoHCI. Virtual reality sickness: a review of causes and measurements. 2020;36(17):1658-82.
40. LaViola Jr JJJASB. A discussion of cybersickness in virtual environments. 2000;32(1):47-56.
41. McHugh N. Measuring and minimizing cybersickness in virtual reality. 2019.
42. Drascic D, Milgram P, editors. Perceptual issues in augmented reality. Stereoscopic displays and virtual reality systems III; 1996: Spie.
43. Watson AB, Yellott JI. A unified formula for light-adapted pupil size. Journal of Vision. 2012;12(10):12-.
44. Sauer Y, Sipatchin A, Wahl S, García García M. Assessment of consumer VR-headsets' objective and subjective field of view (FoV) and its feasibility for visual field testing. Virtual Reality. 2022;26(3):1089-101.
45. William B, Asiedu D, Hermawan A, Luckyarno Y, Yun J-H. Adaptive Foveated Rendering and Offloading in an Edge-Assisted Virtual Reality System. IEEE Access. 2024;12:17308-27.

46. Hsu C-F, Chen A, Hsu C-H, Huang C-Y, Lei C-L, Chen K-T, editors. Is foveated rendering perceivable in virtual reality? Exploring the efficiency and consistency of quality assessment methods. Proceedings of the 25th ACM international conference on multimedia; 2017.
47. Hollander DA, Volpe NJ, Moster ML, Liu GT, Balcer LJ, Judy KD, et al. Use of a portable head mounted perimetry system to assess bedside visual fields. The British journal of ophthalmology. 2000;84(10):1185-90.
48. Phu J, Wang H, Kalloniatis MJO, Optics P. Comparing a head-mounted virtual reality perimeter and the Humphrey Field Analyzer for visual field testing in healthy and glaucoma patients. 2024;44(1):83-95.
49. Bradley C, Ahmed IIK, Samuelson TW, Chaglasian M, Barnebey H, Radcliffe N, et al. Validation of a Wearable Virtual Reality Perimeter for Glaucoma Staging, The NOVA Trial: Novel Virtual Reality Field Assessment. 2024;13(3):10-.
50. Johnson C, Sayed A, McSoley J, Durbin M, Kashem R, Nicklin A, et al. Comparison of Visual Field Test Measurements With a Novel Approach on a Wearable Headset to Standard Automated Perimetry. Journal of glaucoma. 2023;32(8):647-57.
51. Mees L, Upadhyaya S, Kumar P, Kotawala S, Haran S, Rajasekar S, et al. Validation of a head-mounted virtual reality visual field screening device. 2020;29(2):86-91.
52. Stapelfeldt J, Kucur SS, Huber N, Höhn R, Sznitman R. Virtual Reality-Based and Conventional Visual Field Examination Comparison in Healthy and Glaucoma Patients. Translational vision science & technology. 2021;10(12):10.
53. Narang P, Agarwal A, Srinivasan M, Agarwal AJOS. Advanced vision analyzer–virtual reality perimeter: device validation, functional correlation and comparison with humphrey field analyzer. 2021;1(2):100035.
54. Selvan K, Mina M, Abdelmeguid H, Gulsha M, Vincent A, Sarhan A. Virtual reality headsets for perimetry testing: a systematic review. Eye (London, England). 2024;38(6):1041-64.
55. Navascues-Cornago M, Morgan PB, Maldonado-Codina C, Read MLJO, Optics P. Characterisation of blink dynamics using a high-speed infrared imaging system. 2020;40(4):519-28.
56. Nyquist HJTotAIoEE. Certain topics in telegraph transmission theory. 1928;47(2):617-44.
57. Eldar YC, Oppenheim AVJIToSP. Filterbank reconstruction of bandlimited signals from nonuniform and generalized samples. 2000;48(10):2864-75.
58. Schoder V, Himmelmann A, Wilhelm KJC, dermatology e. Preliminary testing for normality: some statistical aspects of a common concept. 2006;31(6):757-61.
59. Solomon SG, Lennie PJNRN. The machinery of colour vision. 2007;8(4):276-86.
60. Zhang X, Kedar S, Lynn MJ, Newman NJ, Biousse V. Homonymous hemianopias: clinical-anatomic correlations in 904 cases. Neurology. 2006;66(6):906-10.

Appendices

Appendix A: AUMC Neuro app supplementary document

Visual Field Stimulation & Visual Field Examination

-Focus points appear on a virtual plane which distance is 2 units (meters) from camera (head)
-Background grid distance is 2.1m from camera
-Focus point black center sphere diameter is 0.1m
-Focus point gaze acceptable range sphere is 0.233m
-Focus point and background grid maintain their relative position and rotation to camera when head rotates

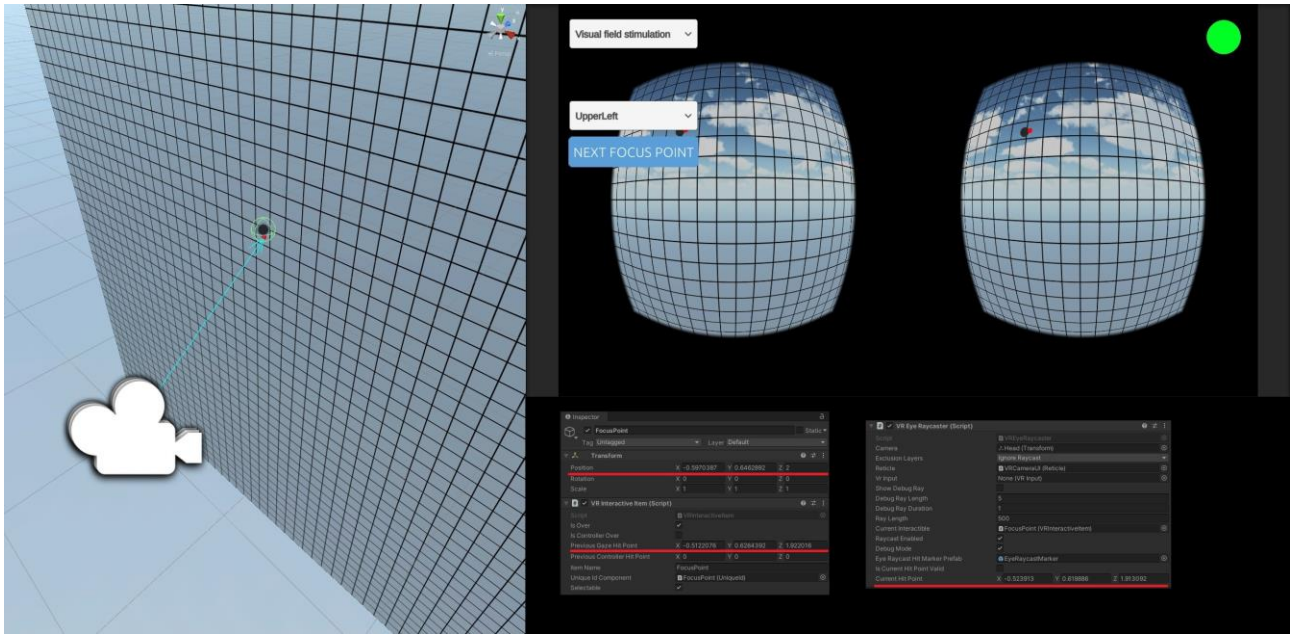

-Focus point position is center of black sphere in world coordinates
-'Previous Gaze hit Point' is last recorded eye-gaze hit point on acceptable range sphere in world coordinates
-'Current Hit Point' is eye-gaze current hit point on acceptable range sphere or on background

-Dots appear 3m from focus point
-Approaching time per dot is 10 seconds
-Approach sequence starts when gaze has been in acceptable range continuously 1 second

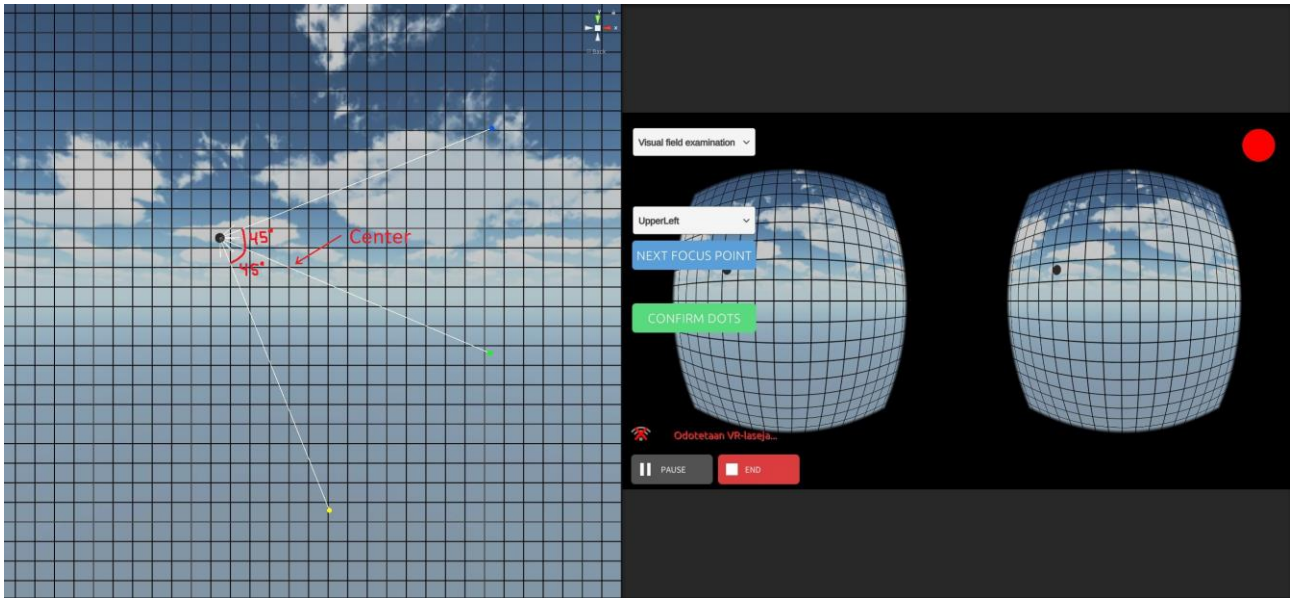

Focus point(s) data is saved on DataRecords.json -file
`"relativePositionToCamera"` = focus point relative position to camera (head)
`"dotConfirmTimeStamps"` = collection of timestamps when 'Confirm dots' -button has been pressed. These timestamps and `"timeStamp"` are relative to test start time i.e. when 'Start' -button has been pressed


```
{
  "$type": "Peili.AUMCNeuro.FocusPointData, Assembly-CSharp",
  "timeStamp": 0.0,
  "totalDuration": 34.7523766,
  "relativePositionToCamera": {
    "x": 0.484980047,
    "y": 0.144276261,
    "z": 2.0
  },
  "visualFieldArea": "MiddleRight",
  "timeDurationFromAppearanceToAcceptableRange": 3.67964959,
  "timeAmountInFosusing": 31.1111736,
  "timeAmountInStabilizing": 0.9757826,
  "acceptableRangeRatio": 0.895224333,
  "dotConfirmTimeStamps": {
    "$type": "System.Collections.Generic.List`1[[System.Single, mscorlib]], mscorlib",
    "$values": [
      9.882411,
      20.3254585,
      30.5797138
    ]
```

```
  }
}
```


Dots world coordinates during test are saved in TrackingData.json -file (`"Dot1"`, `"Dot2"`, `"Dot3"`)
TrackingData.json also contains tracking data for camera (head) (`"VRCamera"`)


```
{
  "$type": "SyncedTransformData, Assembly-CSharp",
  "uniqueId": "Dot1",
  "itemName": "Dot1",
  "timeSinceStartup": 139.952,
  "position": {
    "x": -2.011,
    "y": 2.402,
    "z": 0.441
  },
  "rotation": {
    "x": 0.3047,
    "y": 0.6207,
    "z": 0.3386,
    "w": 0.638
  },
  "scale": {
    "x": 0.05,
    "y": 0.05,
    "z": 0.05
  },
  "velocity": {
    "x": -0.022,
    "y": -0.244,
    "z": 0.009
  },
  "angularVelocity": {
    "x": 0.263,
    "y": -0.011,
    "z": -0.438
  }
},
```


To get dots coordinates during different events, you can compare event timestamps from EventData.json to TrackingData.json

For example to get approaching dot position when 'Confirm dots' -button is pressed
find event types `"Peili.AUMCNeuro.ConfirmDots, Assembly-Csharp"` in EventData.json and get corresponding coordinates from TrackingData.json.

If you need to compare that to eye-gaze ray, you can get that from EyeTrackingData.json -file
(`"Peili.EyeTrackingDataPoint, Assembly-Csharp"` `"worldGazeRay"`)

Boston naming
-Images appear on a plane which distance is 2 units (meters) from camera (head)
-Image plane size is 1.13m x 0.85m
-Image plane maintains it's relative position and rotation to camera when head rotates
-'Current Hit Point' is eye-gaze current hit point on image plane

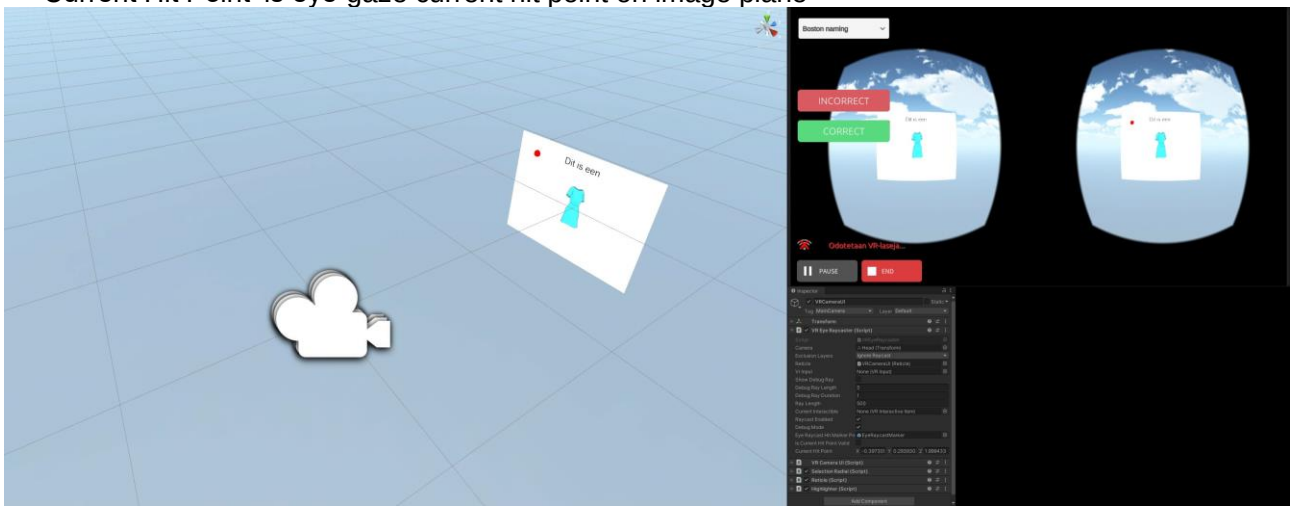

-Naming data is saved on DataRecords.json -file
`"correct"` and `"incorrectType"` are relevant only if `"evaluated"` is true
`"timeStamp"` is relative to test start time i.e. when 'Start' -button has been pressed


```
{
  "$type": "Peili.AUMCNeuro.BostonNamingTargetData, Assembly-CSharp",
  "name": "Complete set_260 Duffau aanbiedingrandom (1)_Sivu_083",
  "targetType": "Image",
  "timeStamp": 0.0,
  "duration": 4.0,
  "evaluated": false,
  "correct": false,
  "incorrectType": "Anomia"
},
```


Data files

DataRecords.json	Data records of head & controller movements and collections of FocusPoint & Boston Naming -target data
EventData.json	Event data sent between tablet and headset
EyeTrackingData.json	Eye tracking gaze data. "localGazeRay" is camera relative gaze and "worldGazeRay" is eye gaze in world coordinates
EyeTrackingValidationResults.json	Eye tracking validation data
Results.txt	Summary of DataRecords
TrackingData.json	Tracking data of head and dots in world coordinates ("VRCamera", "Dot1", "Dot2", "Dot3")

Appendix B: Manual for Peili app

In advance/Installation:

- **Check battery and internet connection.**
  Explanatory video if tablet has issues with connecting to WiFi:
  https://www.youtube.com/watch?v=SNZd2NLF76w&t=164s
  In short: (consider restarting between every step):
  1. (Re)set the time manually in the tablet's settings
  2. Follow and fill in:
  Settings – Connections – Wi-Fi – Gear icon next to the network – Advanced – IP Settings – Static – DNS1 = 8.8.8.8 DNS2 = 8.8.4.4

  [Dutch] Instellingen – verbindingen – wifi – tandwieltje naast netwerk – geavanceerd – IP instellingen – statisch – DNS1 = 8.8.8.8 DNS2 = 8.8.4.4

  3. Sometimes also check:
  Settings – Developer Options – Wi-Fi Scan Throttling should be enabled.
  [Dutch] Instellingen – ontwikkelaarsopties – Beperking wifiscan moet aanstaan.

- Tablet needs at least **~40% battery** percentage and **PICO VRH > 60% battery** percentage
- If the headset shows gaming boundaries upon startup, first select "static" and set them up. However, we want these turned off for the test (so the headset can be passed between users). To turn them off, follow these steps: Settings → General → Playing Boundaries → Shut Off Completely (this option is only available if the headset is in developer mode).
  - To enable developer mode: Go to Settings → General → About → Keep clicking on the software version field until the developer option appears at the bottom of the left navigation pane. (8+ times fast clicking)

Manual for execution of the test on the Peili

0. Explain the procedure:

- Testing the visual field with a VR headset.
- A grid will appear on the headset's display. A black circle will appear, and the participant will be asked to keep looking at the focus point.
- Shortly afterward, a dot will slowly enter the screen from the opposite side, moving toward the displayed focus point. When the participant sees the dot, they should say "DOT" (and press a button on the controller).
- The researcher will record this on the tablet. Once the dot reaches the focus point, a new dot will slowly appear on the screen.
- For each focus point, three dots will appear in succession. This process will be repeated for several focus points.
- The focus points will be displayed in different locations.
- Please note:

- Please indicate whenever the headset does not feel right or is bothering you.
- The headset can be removed at any time; we will need to start over, but that's not a problem.
- For reliable results, it is important that the participant continues to look at the focus point.

1. Start tablet + open Peili app on tablet:

➔ Check battery + internet connection

2. Start bril and controller:

➔ Check battery + internet connection

3. Open the Peili app on the VRH until the virtual waiting room is shown. Then hand VRH to participant.
   a. Instructions on the app are in English, if the participant is Dutch, please translate it for them.

4. This happens step-by-step on the VRH:

VRH/Pt sees	**Tablet shows**	**Notes/NB:**
Waiting room.	AUMC Next exercise with buttons: - Play - **Calibrate eyetracking**	
START CALIBRATION	**START CALIBRATION**	**START CALIBRATION**
Grey screen with blue dot "follow point with gaze"	Settings: Automatic sequence aan Number of Points: 5 Success threshold: 2 2 buttons: - **Start calibration** - Start validation	Calibration is always 5-point calibration, validation can be 5 or 9.
Sometimes the VRH will ask the patient to adjust th headset.	Grey screen	Generally, this can be fixed by tightening the headset. Sometimes the patient has to direct their chin more to their chest. Adjustments must be made slow, this way the headset will show a figure that indicates how it should be readjusted.

Optional: headset will not start calibration	Screen stays grey	Turn Pico device on and off. You can also try performing an extra calibration in the homescreen. It says "Tobii or Unity calibration"on the right side of the menu.
Patient is shown the 5-dot calibration. After all 5 dots have been looked at, the patient sees a tick.	Calibration procedure is not visualised correctly, it takes about 10 to 15 seconds. When calibration is finished, the gaze is visualised on the screen of the tablet. Then, you can **start validation**	You can consider asking the patient to indicate when they see the tick.
Patient performs validation. After finalizing it, they will see the validity score (almost always 100%)	Validation takes around the same time, but now you can follow it on the tablet and you know when it is done. When it is done, you can see the validation results on the tablet screen, if you think the error is small enough, click **accept.**	If validation score is low, consider restarting with calibration and then validation.
START TEST	**START TEST**	**START TEST**
Wating room	AUMC Next exercise with buttons: - **Play** - Calibrate eye-tracking	
Grid in front of blue sky with clouds	Settings: - **Visual field examination** - Choose the position of your focuspoint - **START**	
Grid/sky/Focus Point	The top right shows a red or green round shape. This indicates if the patient is correctly gzaing at the focus point Rectsboven zie je of ze naar fp kijken (green = yes; red = no)	Whenever you see that they are not gazing towards the focus point, remind the participant or patient to maintain their gaze upon the black dot.

While the dots are approaching, you can already choose or determine the area where you want to show the next focus point. This is changed when you click "next focus point".

5. Save the data: exit and save data.
6. Export data from VRH to your laptop

➔ Connect Pico with laptop via usb.
➔ Turn on headset to allow your laptop to recognize it.
➔ Go to:
This PC\MTP USB Device\Internal shared storage\Android\data\com.peilivision.researchVR\files\ExerciseSessionsData
➔ Copy and paste the data set to your own laptop on a designated location.

Appendix C: Overview of isopters of all datasets from healthy volunteer.

Dataset 1

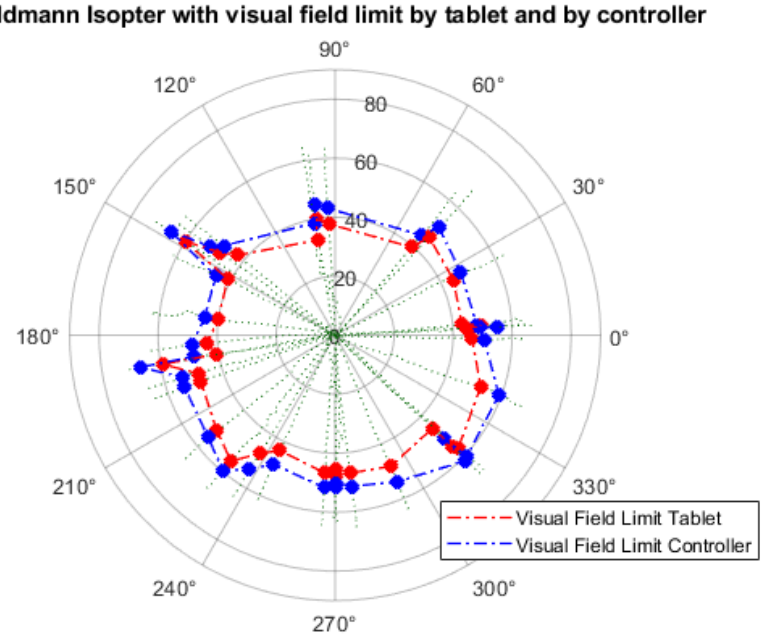

Dataset 2

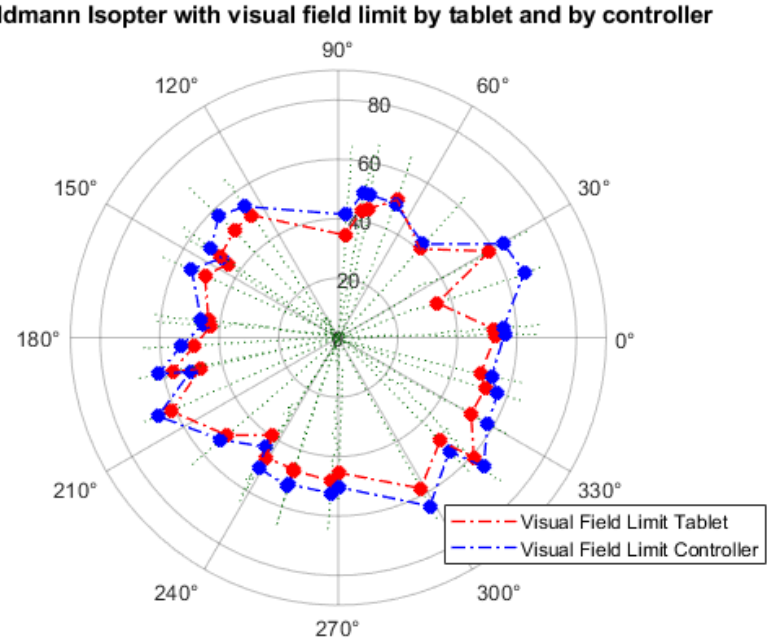

Dataset 3

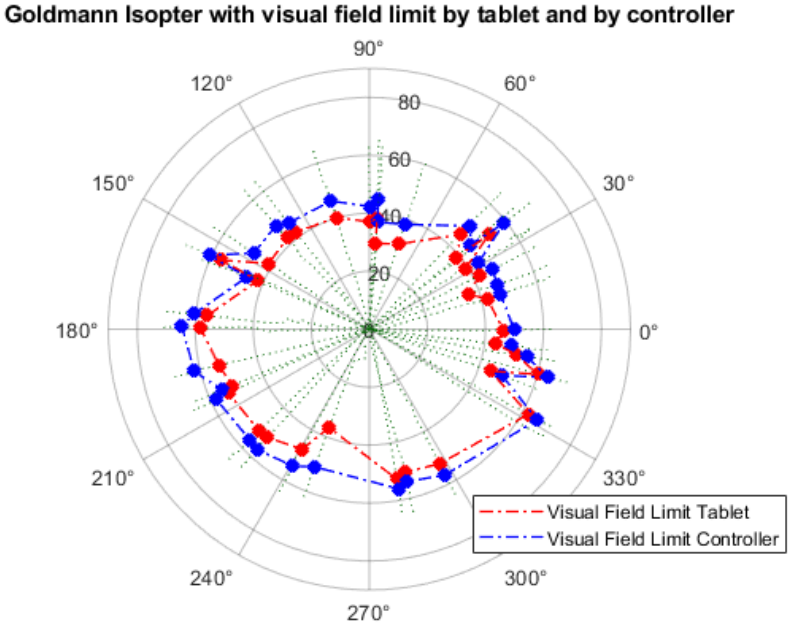

Dataset 4

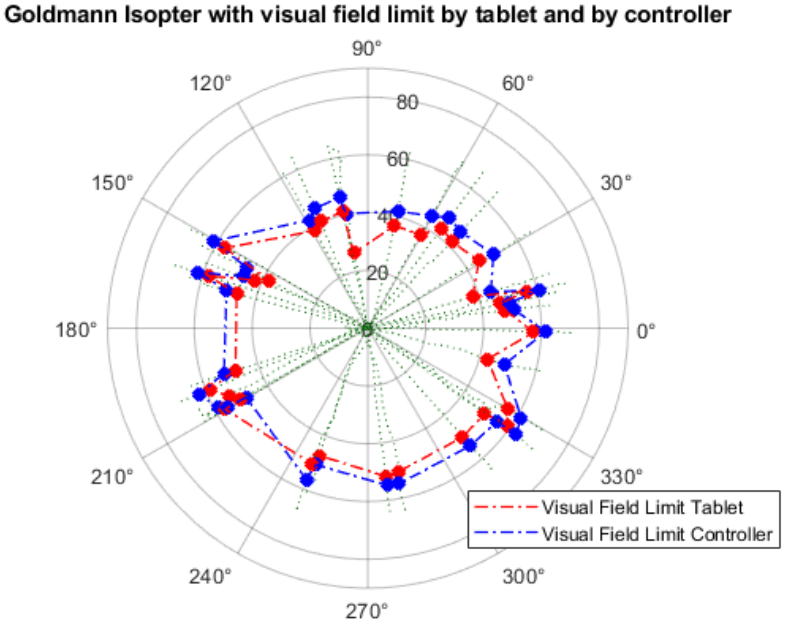

Dataset 5

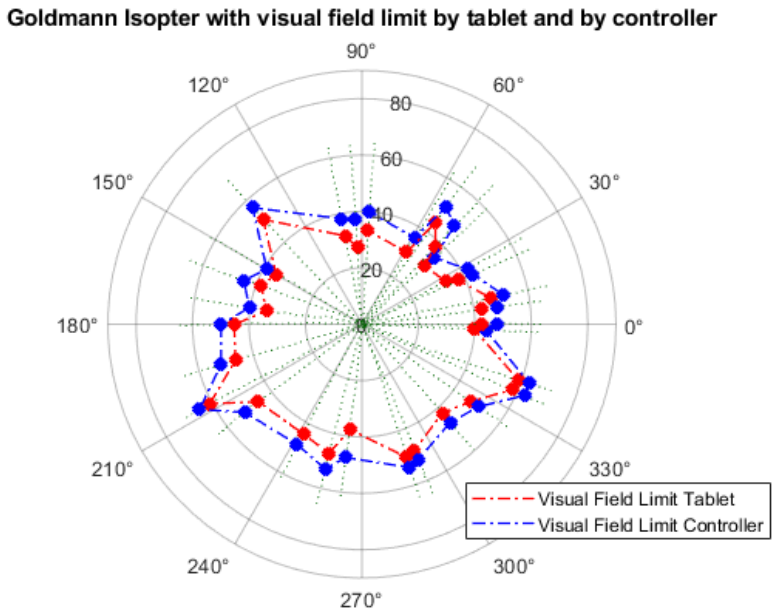

Datasett 6

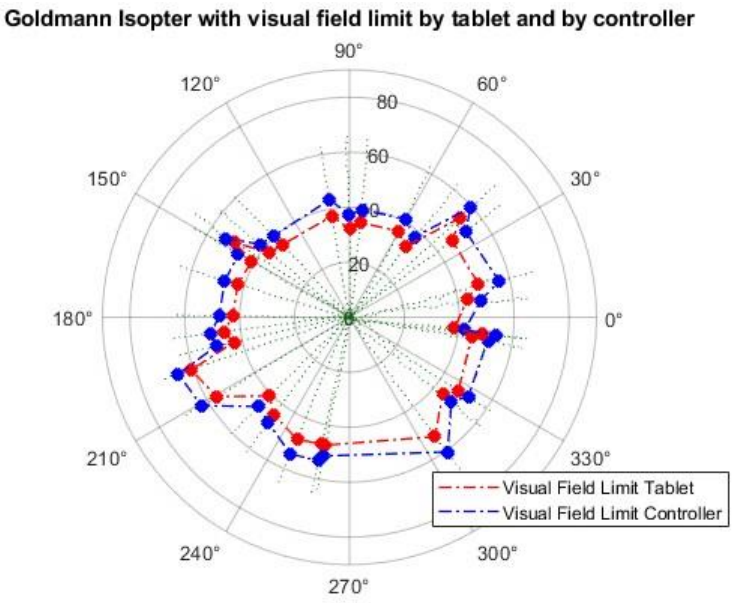

Dataset 7

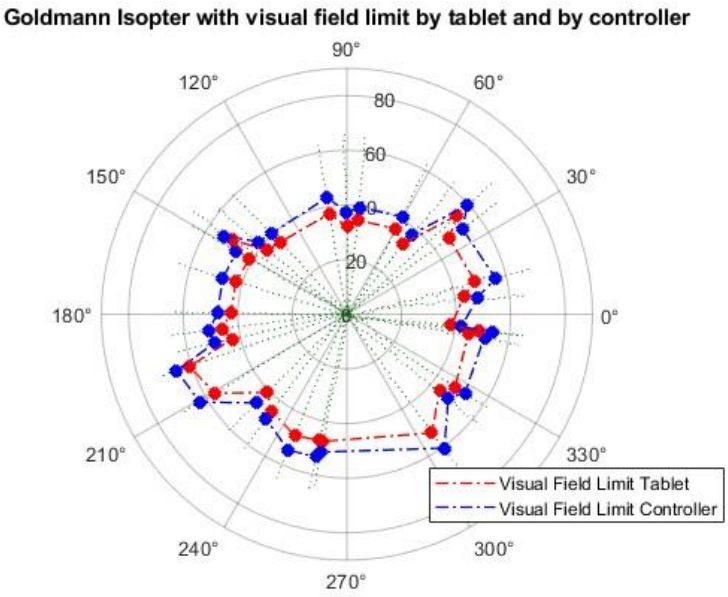

Dataset 8

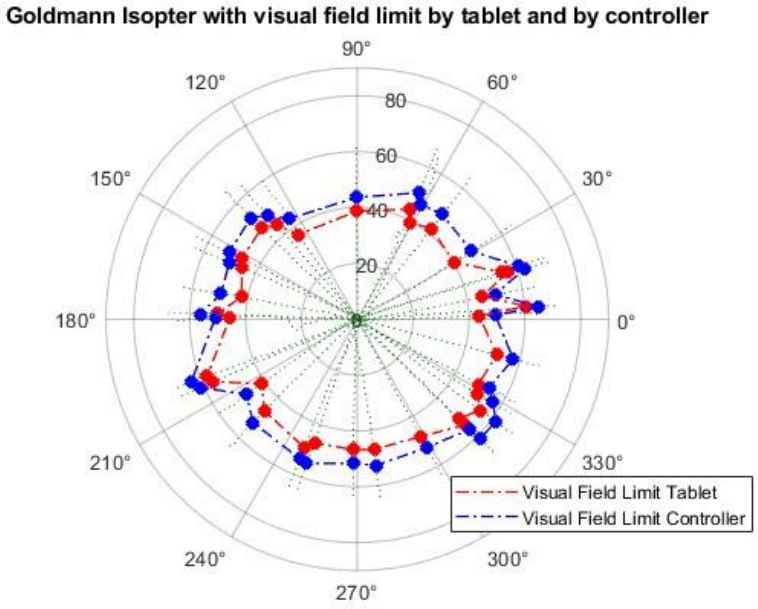

Dataset 9

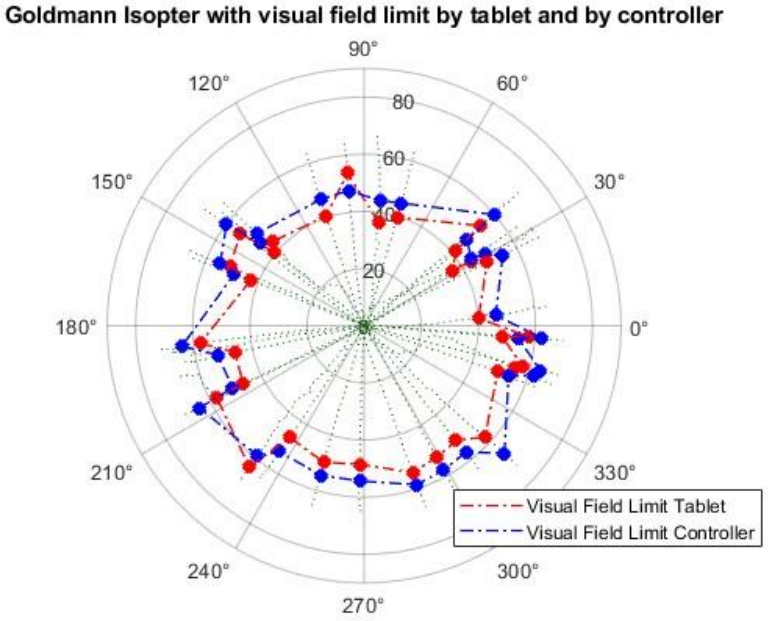

Dataset 10